Bioorganic Chemistry 104 (2020) 104255

Contents lists available at ScienceDirect

Bioorganic Chemistry

journal homepage: www.elsevier.com/locate/bioorg

Design, efficient synthesis, docking studies, and anticancer evaluation of new quinoxalines as potential intercalative Topo II inhibitors and apoptosis inducers

Eslam M. Abbass[a], Ali Kh. Khalil[a], Mohamed M. Mohamed[a], Ibrahim H. Eissa[b,*], Abeer M. El-Naggar[a,*]

[a] Chemistry Department, Faculty of Science, Ain Shams University, Abbassia, Cairo 11566, Egypt
[b] Pharmaceutical Medicinal Chemistry & Drug Design Department, Faculty of Pharmacy (Boys), Al-Azhar University, Cairo 11884, Egypt

ARTICLE INFO

Keywords:
Anticancer
Apoptosis
DNA-intercalator
Molecular docking
Quinoxaline
Topoisomerase II

ABSTRACT

As an extension for our earlier effort in the field of discovery of anticancer agents acting on DNA and Topo II, eighteen quinoxaline derivatives were designed and synthesized. Such members were designed to possess the main essential pharmacophoric features of DNA intercalators. The cytotoxic potential of the synthesized compounds was assessed against a group of human cancer cell lines (HCT-116, HepG2, and MCF-7). Doxorubicin as potential intercalative Topo II inhibitor, was used as a positive reference. In general, compounds **12**, **15**, **19**, **21**, and **22** showed promising anti-proliferative activities against the three cell lines with IC_{50} values ranging from 2.81 to 10.23 μM. The cytotoxicities of the most active compounds against normal human cells (WI-38) were evaluated, and the results revealed that these compounds have low toxicity. Further examination for the most active anti-proliferative members as Topo II inhibitors was also performed, showing a narrow range of the inhibitory activities (from 0.45 to 1.06 μM). In addition, DNA/methyl green assay was carried out to evaluate DNA-binding potential of such compounds. The results indicated that these compounds have strong to moderate DNA-binding affinities ranging from 33.48 to 51.23 μM. Further studies exhibited the capability of compound **22** to induce apoptosis in HepG2 cells and can arrest growth of such cells at G2/M phase. Also, compound **22** produced a significant increase in the level of caspase- 3 (10 folds) and caspase-9 (7 folds) compared to the control cells. Molecular docking studies were also conducted to investigate possible binding interactions between the target compounds and the DNA-Topo II complex.

1. Introduction

Most anticancer drugs are pronounced to cause many adverse effects [1]. Now, there an urgent need to develop anticancer agents with enhanced therapeutic index. Several anticancer drugs exhibit their clinical efficacy by causing DNA damage. These drugs can consequently push cancer cells into apoptosis [2]. DNA intercalating agents are considered as one of the most well-known group of DNA damage [3]. Also, the class of topoisomerase II inhibitors is one of the most famous DNA damaging agents [4]. Additionally, DNA intercalators and topoisomerase II inhibitors are renowned apoptosis inducers [5]. Therefore, targeting DNA via DNA intercalators and topoisomerase II inhibitors has the potential for more effective therapies to improve cancer patient survival [6].

DNA intercalators are planar aromatic compounds that can insert themselves between DNA base pairs without replacing the original nitrogenous bases [7]. At the site of intercalation, the hydrogen bonds between the nitrogenous bases remain unbroken [8]. DNA intercalators can stabilize themselves at the site of insertion via π-stacking between the aromatic part of the intercalator and the nitrogenous bases [9]. Additionally, there are many types of chemical bonds which facilitate intercalation process such as hydrophobic, van der Waals, electrostatic, and entropic interactions [10]. The ability of DNA intercalators to interact with DNA generates their potential therapeutic applications as anticancer agents [5].

Topoisomerase II is a crucial cellular enzyme that modifies DNA topology. This enzyme is involved in several metabolic processes such as chromosome replication, recombination, transcription, and segregation. It works by breaking the double stranded-DNA and then resealing the breaks that have been produced [11].

* Corresponding authors.
E-mail addresses: Ibrahimeissa@azhar.edu.eg (I.H. Eissa), elsayedam@sci.asu.edu.eg (A.M. El-Naggar).

https://doi.org/10.1016/j.bioorg.2020.104255
Received 1 June 2020; Received in revised form 15 August 2020; Accepted 28 August 2020
Available online 02 September 2020

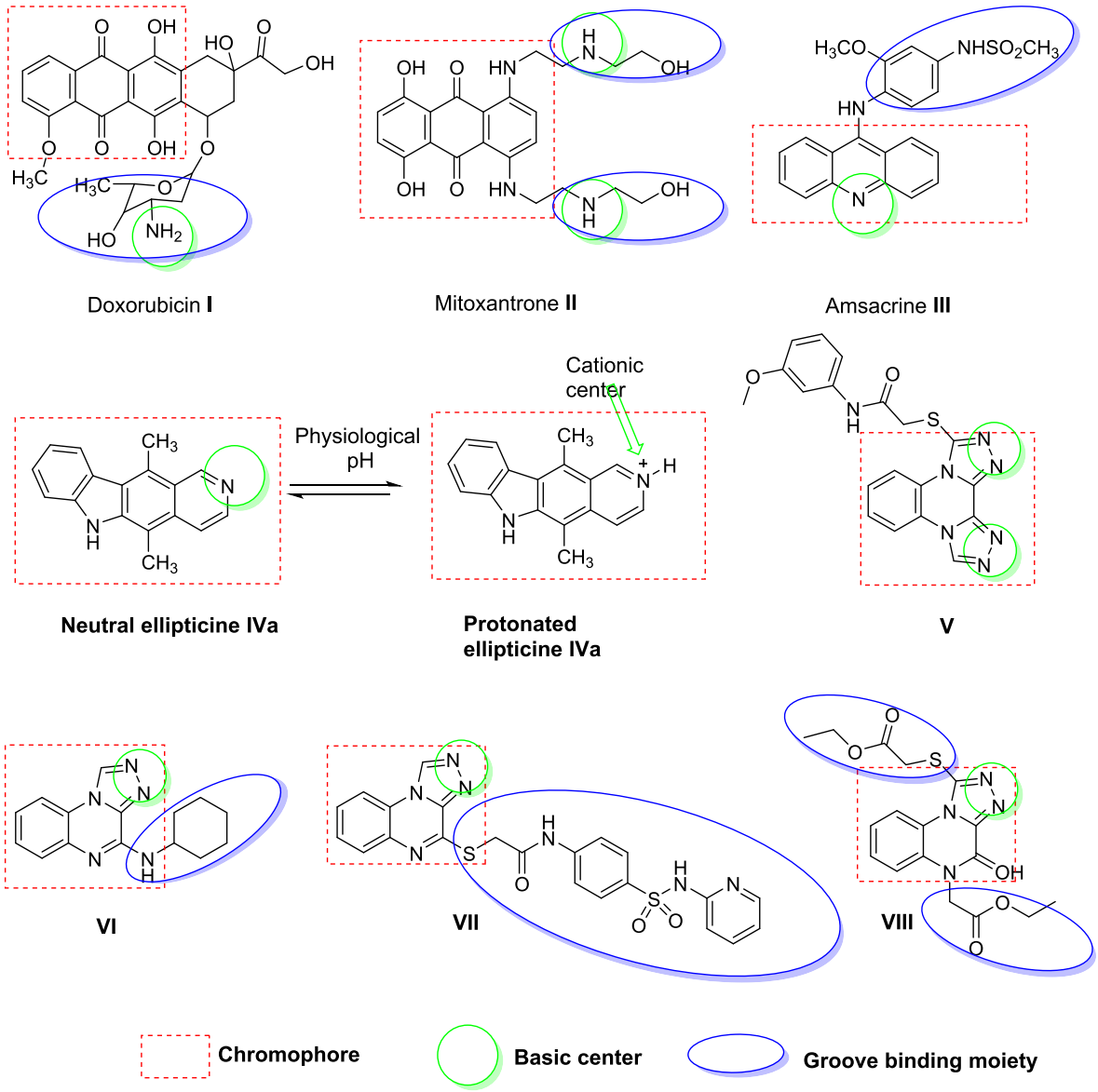

Fig. 1. Some reported DNA intercalators and their basic pharmacophoric features.

Topo II targeting anticancer agents comprise intercalating drugs that interfere with cleavage and rejoining abilities of the enzyme. Such interference takes place through trapping the cleavable complex and thus increasing the half-life of the transient DNA breaks catalyzed by Topo II. This category of drugs is called Topo II poisons as they transform the Topo II into a DNA-damaging factor [6,12]. Due to their promising antitumor activities, the intercalative Topo II poisons have attracted particular attention [7]. Many intercalative Topo II poisons are either already used as an anticancer drug or still under clinical trials (e.g., doxorubicin **I** [13], mitoxantrone **II** [14], amsacrine **III** [15], and ellipticine **IV** [16]. Additionally, for several years, our research team introduced promising some intercalative Topo II poisons as compounds **V, VI, VII,** and **VIII**. Some of these compounds were reported to induce apoptosis [4,17] (Fig. 1).

Depending on the fore mentioned reports, and in continuation of our team previous works in the field of design and synthesis of new anticancer agents [18–22], in particular DNA intercalators and Topo II inhibitors [4,17,23,24], we reported the design and synthesis of new intercalative Topo II poisons. The designed compounds are quinoxaline derivatives having the main pharmacophoric features of DNA intercalators.

1.1. The rationale of molecular design

Studying the reported structure-activity relationship of DNA intercalators, it was found that they have three essential pharmacophoric features, i) chromophore moiety which is a planar polyaromatic structure with higher priority for three or four fused aromatic system [25]. ii) A cationic center, which can interact with the negatively charged phosphate moiety of DNA. The cationic centers are basic amino atoms which can undergo protonation in physiological pH [16], iii) Groove binding side chain, which occupies the DNA minor groove, increasing stability of binding [26–28] (Fig. 2).

The our previously synthesized compounds **VII** and **VIII** were reported to have promising antiproliferative and Topo II inhibitory activities. Compound **VII** is a classical DNA-intercalator, while compound **VIII** is a threading DNA-intercalator (Fig. 1) [17]. In the current work, these compounds were selected to be lead structures in the synthesis of new derivatives. The rationale of our molecular design depended on the lead modification of such compounds to get two scaffolds of new classical DNA-intercalators. The first scaffold is [1,2,4]triazolo[4,3-*a*] quinoxalin-4(5*H*)-one, which consists of three fused aromatic system. Depending on the ring opening strategy of drug design, the second

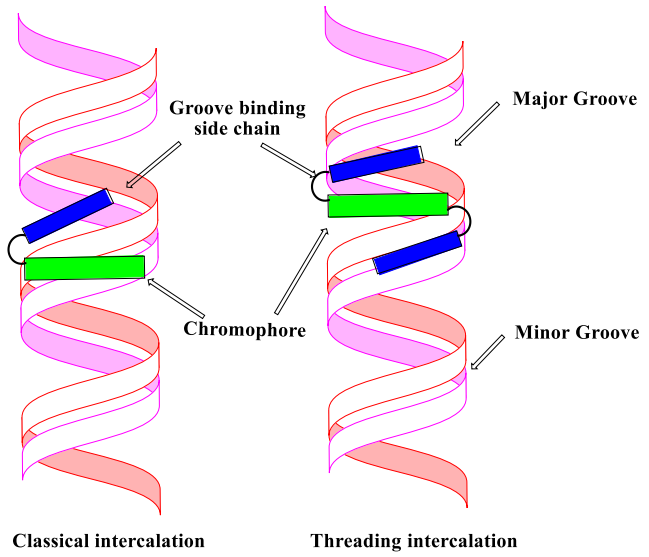

Fig. 2. Schematic representation of classical and threading DNA intercalation (based on Ref. [17]).

scaffold (quinoxalin-2(1*H*)-one) was obtained, consisting of two fused aromatic system. In each scaffold, many chemical substituents with variant hydrophobic, electronic, and bulky effects were used to study the structure-activity relationship (Fig. 3).

2. Result and discussion

2.1. Chemistry

As a continuation of our research efforts towards the development of simple and efficient synthetic methodologies for synthesis of new heterocyclic compounds with anticipated pharmaceutical activities [24,29–32]. Herein, a green approach was applied for constructing some quinoxaline derivatives which in turn was evaluated as plausible anticancer agents. Initially, the quinoxaline-2,3-dione **3** was synthesized by reflux of *o*-phenylenediamine with oxalic acid in 4N HCl [24]. Reaction of compound **3** with hydrazine hydrate gave 3-hydrazinoquinoxaline-2(1*H*)-one **4** as a key compound for further synthetic pathways [33].

Depending on both conventional and microwave conditions, compound **4** was treated with different carbonyl compounds namely, 2-acetylthiophene, 2-acetylfuran, 4-acetylbiphenyl, 4-methylacetophenone, 6-chloro-4-oxo-4*H*-chromene-3-carbaldehyde, 1,3-diphenyl-1*H*-pyrazole-4-carbaldehyde, 1-indanone, and cyclohexanone in ethanol to furnish the corresponding hydrazone derivatives **5–12**, respectively (Scheme 1).

The IR spectra of compounds **5–12** demonstrated stretching bands at a range of 1662–1698 cm^{-1} attributed to C=O groups. In addition, all Schiff bases **5–12** showed the disappearance of NH_2 band of the hydrazinyl group presented in compound **4**. Further support for their assigned structures was gained from their ^1H NMR spectra, which revealed D_2O exchangeable singlet signals in a range of δ 9.30–11.59 ppm attributed to NH groups. The values for NH, integration values for methyl group protons and aromatic protons of compounds **5–8** showed the existence of the *E/Z* mixture with a ratio of 54: 46. The methine proton (CH=N) in both compounds **9** and **10** are shown at δ 8.6–9.04 ppm range which ascertained their structures. Additionally, ^1H NMR of compound **11** showed triplet bands at range of δ 2.98–3.05 ppm corresponding to two methylene groups in indanone moiety.

Cyclocondensation of the hydrazinyl derivative **4** with different electrophilic species such as formic acid, acetic acid and carbon disulphide was carried out under conventional, microwave and ultrasonic conditions afford the corresponding triazole derivatives **13–15** (Scheme 2). It was observed that the non-classical conditions enhanced the yield of the target products with shorter time than conventional condition as shown in the comparative study depicted in Table 1.

The IR spectra of compounds **13–15** showed the disappearance of NH_2 band of hydrazinyl moiety of compound **4** and the appearance of stretching bands at a range of 1673–1700 cm^{-1} corresponding to C=O groups. ^1H NMR of compounds **13–15** showed exchangeable singlet signals at range of δ 11.98–12.01 ppm corresponding to NH group of quinoxaline ring, singlet signal at δ 9.86 ppm due to CH of triazole ring of compound **13,** singlet signals at δ 2.97 ppm corresponding to CH_3 of compound **14** and an exchangeable singlet signal at δ 14.63 ppm attributed to SH group of quinoxaline derivative **15.**

Reactions **of 15** with different halide derivatives namely, ethyl chloroacetate, chloroacetic acid, chloroacetone, chloroacetyl chloride, 2-chloro-*N*-(*p*-tolyl) acetamide, and furoyl chloride in DMF under basic condition using few drops of triethyl amine in both conventional and green conditions to afford the final compounds **14–20** (Scheme 3). As shown in Table 1, the modified condition provided better yield and shorter time than conventional method.

The spectral data were fit with the assigned structures of compounds **16–22.** For compound **16**, the IR spectrum demonstrated a stretching band at 1733 cm^{-1} corresponding to C=O of the ester. Moreover, ^1H NMR spectrum revealed the appearance of new signals at δ 1.15, 4.09 and 4.37 ppm corresponding to CH_2-CH_3 and CH_2 groups, respectively. In case of compound **17**, the IR spectrum showed stretching bands at 3438, 3137 cm^{-1} corresponding to OH and NH groups, respectively. Its ^1H NMR spectrum showed a singlet signal at δ 4.10 ppm corresponding to CH_2 group. IR spectrum of compound **18** exhibited a band at 1711 cm^{-1} attributed to C=O group while its ^1H NMR showed the appearance of singlet signals at δ 2.30, 4.56 ppm attributed to CH_3, CH_2 respectively. The IR spectrum of compound **19** showed the appearance of a stretching band at 1671 cm^{-1} corresponding to C=O of acetyl group. In addition, its ^1H NMR spectrum showed a singlet signal at δ 4.32 ppm corresponding to CH_2 group. For compound **20**, the IR spectrum showed stretching bands at 1677, 1685 cm^{-1} corresponding to mechanical coupling of two C=O of acetyl acetone moiety while ^1H NMR spectrum showed singlet signals at δ 2.37, 4.56 ppm corresponding to CH_3, CH respectively. For compound **21**, the IR spectrum exhibited a stretching band 1674 cm^{-1} corresponding to C=O, ^1H NMR showed a singlet signals at δ 2.24 and 4.45 ppm corresponding to CH_3 and CH_2, respectively and an exchangeable singlet signal at 12.05 ppm corresponding to NH. Finally, the IR spectrum of compound **22** showed a stretching band at 1688 cm^{-1} corresponding to C=O.

2.2. Biological evaluation

2.2.1. In vitro anti-proliferative activity

In vitro cytotoxic activity of the synthesized compounds were evaluated against colorectal carcinoma (HCT-116), hepatocellular carcinoma (HepG2), and breast cancer (MCF-7). A standard MTT assay [34–36] was performed, utilizing doxorubicin as a positive control. For each compound, the growth inhibitory concentration (IC_{50}) values were determined and reported in Table 2.

The synthesized compounds showed different grades of anti-proliferative potency, ranging from very strong, strong, moderate to weak.

In general, compounds **15**, **19**, and **22** showed very strong anti-proliferative activities against the three cell lines with IC_{50} values ranging from 2.81 to 10.23 μM. Doxorubicin showed IC_{50} values of 4.50, 4.17 and 5.23 μM against HCT-116, HepG2, and MCF-7, respectively.

For compound **15,** it showed IC_{50} values of 7.70, 5.98 and 6.35 μM against HCT-116, HepG2, and MCF-7, respectively. While compound **19,** exhibited IC_{50} values of 9.61, 3.48 and 5.16 μM against HCT-116, HepG2, and MCF-7, respectively. Also, compound **22,** showed IC_{50}

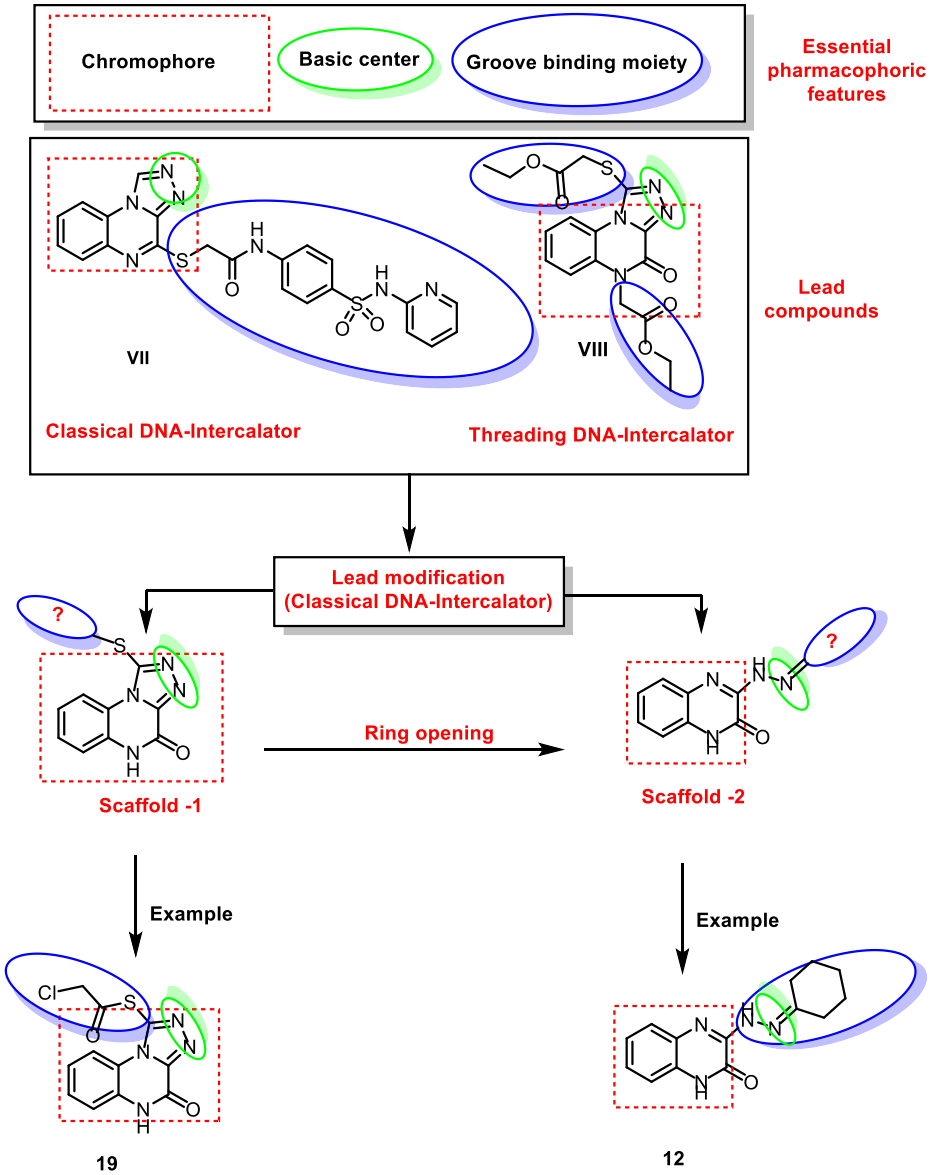

Fig. 3. Rationale of molecular design of new DNA-intercalators.

values of 10.23, 2.81 and 7.28 μM against HCT-116, HepG2, and MCF-7, respectively. It is noteworthy that the inhibitory activity of compounds **19**, and **22** were higher than that of the reference drug against HepG2 cell with IC_{50} values of 3.48 and 2.81 μM, respectively. Compound **12** showed very strong anti-proliferative activities against only HepG2 and MCF-7 cells with IC_{50} values of 4.67 to 9.17 μM, respectively. Compounds **6** and **21** showed very strong anti-proliferative activities against only HepG2 cells with IC_{50} values of 9.85 to 8.07 μM, respectively.

Additionally, many compounds as **5, 6, 8, 12, 20,** and **21** demonstrated strong anti-proliferative activities against at least one cell line with IC_{50} values ranging from 12.86 to 20.39 μM. Compounds **5, 7, 8, 10, 11, 18,** and **20** displayed moderate anti-proliferative activities against at least two cell lines with IC_{50} values ranging from 21.12 to 48.76 μM.

On the other hand, compounds **9, 13, 14, 16,** and **17** displayed weak anti-proliferative activities against at least two cell lines with IC_{50} values ranging from 51.92 to 91.46 μM. Finally, compound **14** showed no activity against MCF-7 cell line.

2.2.2. *In vitro cytotoxicity against human normal cell*

The cytotoxicities of the most active compounds (**12**, **15**, **19**, **21**, and **22)** against WI-38 cell line (normal human lung fibroblasts) were evaluated *in vitro*. The results revealed that the tested compounds have low toxicity against WI-38 with IC_{50} values ranging from 38.92 to 81.20 μM. The cytotoxicity of the tested compounds against the cancer cell lines was from 2.81 to 15.86 μM.

Compounds **12**, **15**, **19**, **21**, and **22** are respectively, 17.39, 10.75, 16.42, 4.82, and 15.21 fold times more toxic in hepatocellular carcinoma (HepG2, the most sensitive cells) than in WI-38 cells.

2.2.3. *Topoisomerase II inhibitory activity*

The most active cytotoxic members (**12**, **15**, **19**, **21**, and **22)** were further evaluated for their effect as Topo II inhibitors. The catalytic inhibition of Topo II was performed using the reported procedure designated by Patra et al. [37]. Camptothecin as a potent Topo II inhibitor, was utilized as a positive control in such teste. The results of Topo II inhibition were reported in Table 3 as IC_{50} values calculated from the concentration-inhibition response curve.

As presented in Table 3, all the examined members could inhibit the Topo II activity. These compounds showed a narrow range of the

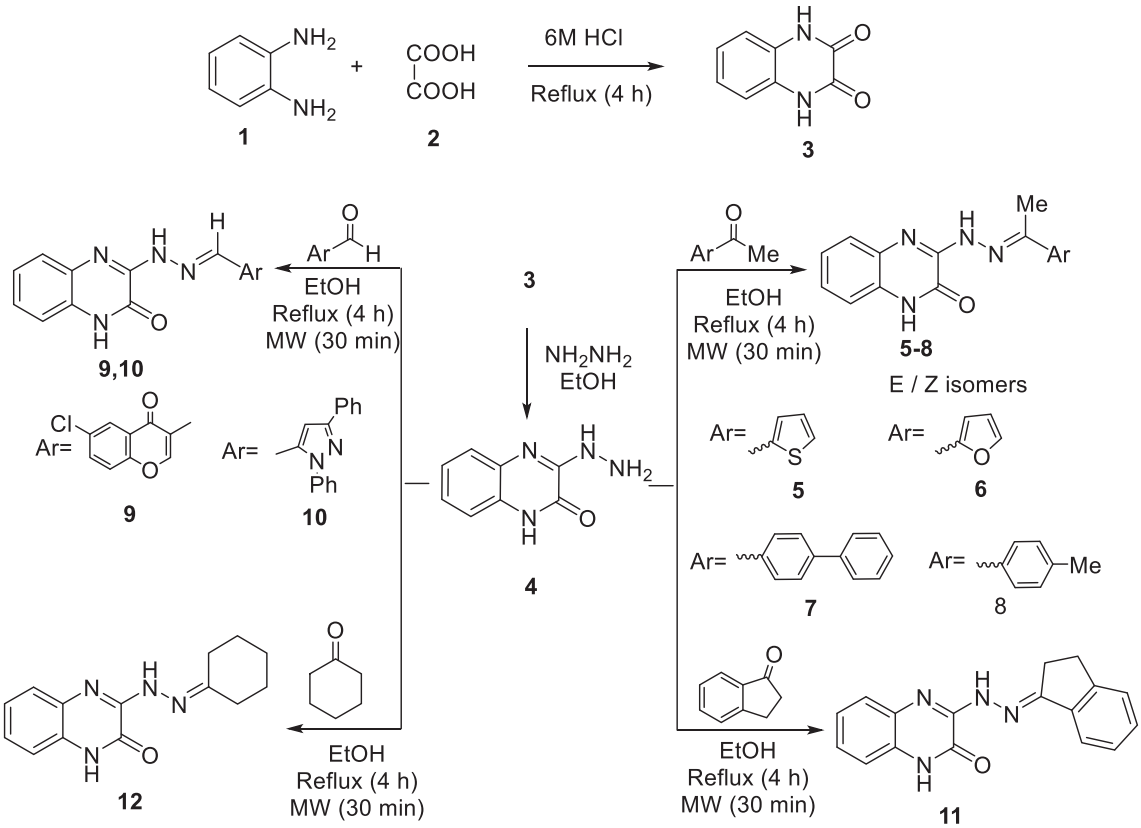

Scheme 1. Synthesis of the target compounds **3–12.**

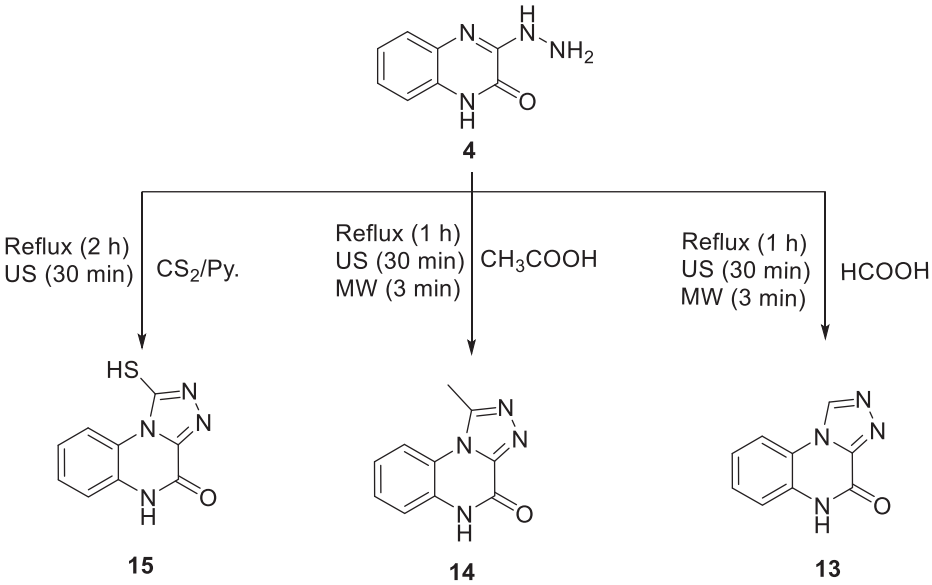

Scheme 2. Synthesis of the target compounds **13–15.**

inhibitory activities (from 0.45 to 1.06 μM). These activities are ranging from excellent, good to moderate comparing to the reference drug (IC_{50} = 0.44 μM). Compounds **21** and **22** showed excellent inhibitory activities with IC_{50} values of 0.45 and 0.52 μM, respectively. Additionally, compounds **12** and **19** exhibited good inhibitory activities with IC_{50} values of 0.89 and 0.62 μM, respectively), Moreover, compound **15** exhibited moderate inhibitory activity, with IC_{50} value of 1.06 μM.

2.2.4. DNA intercalation assay (DNA/methyl green assay)

The most promising derivatives (**12**, **15**, **19**, **21**, and **22)** were subjected to DNA/methyl green assay to evaluate their DNA-binding affinities. The reported method described by Burre et al. [38] was utilized in this test, using doxorubicin as a positive control. The results of DNA-binding affinities were reported in Table 3 as IC_{50} values calculated from the concentration-inhibition response curve.

The results indicated that the tested compounds showed strong to moderate DNA-binding affinities, comparing to doxorubicin

Table 1
Reaction time and yield of conventional, ultrasonic, and microwave assisted synthesis of the synthesized compounds.

Comp.	Time (min)			Yield (%)		
	MW[a]	US[a]	C[a]	MW[a]	US[a]	C[a]
5	30	–	240	85	–	72
6	30	–	240	83	–	73
7	30	–	240	82	–	67
8	30	–	240	89	–	70
9	30	–	240	93	–	78
10	30	–	240	92	–	76
11	30	–	240	90	–	74
12	30	–	240	91	–	77
13	3	30	60	93	84	88
14	3	30	60	90	80	85
15	–	30	120	–	82	87
16	4	60	180	85	74	78
17	4	60	140	89	82	84
18	4	60	180	88	77	80
19	4	60	180	87	75	81
20	4	60	180	89	82	84
21	4	60	180	90	85	85
22	4	60	180	86	80	81

[a] C: conventional, US: ultrasonic, MW: microwave.

(IC_{50} = 31.22 μM). The range of DNA-binding affinities is from 33.48 to 51.23 μM.

Compounds **15** and **19** exhibited IC_{50} values of 37.06 and 33.48 μM, respectively. These compounds are 0.84 and 0.93 times as active as doxorubicin, respectively. Compounds **12**, **21**, and **22** showed

Table 2
In vitro anti-proliferative activities of the tested compounds.

Comp.	IC_{50} (μM)[a]			
	HCT-116	HepG2	MCF-7	WI-38
5	28.35 ± 2.2	15.31 ± 1.4	30.48 ± 2.1	NT[a]
6	20.39 ± 1.6	9.85 ± 0.8	17.08 ± 1.4	NT[a]
7	39.02 ± 2.7	24.69 ± 1.9	44.14 ± 2.8	NT[a]
8	25.71 ± 1.9	13.14 ± 1.2	21.12 ± 1.8	NT[a]
9	66.27 ± 3.7	57.04 ± 3.4	74.60 ± 4.1	NT[a]
10	42.87 ± 3.2	48.76 ± 3.0	58.31 ± 3.6	NT[a]
11	32.38 ± 2.4	21.53 ± 1.9	38.27 ± 2.4	NT[a]
12	15.10 ± 1.3	4.67 ± 0.3	9.17 ± 0.8	81.20 ± 4.1
13	84.55 ± 4.6	65.25 ± 3.6	81.72 ± 4.5	NT[b]
14	91.46 ± 4.9	76.54 ± 4.1	NA[c]	NT[b]
15	7.70 ± 0.5	5.98 ± 0.3	6.35 ± 0.5	64.28 ± 3.7
16	72.17 ± 4.0	43.40 ± 2.7	51.92 ± 3.5	NT[b]
17	61.42 ± 3.6	52.30 ± 3.3	68.04 ± 3.8	NT[b]
18	69.20 ± 3.9	34.18 ± 2.3	47.50 ± 3.2	NT[b]
19	9.61 ± 0.8	3.48 ± 0.2	5.16 ± 0.4	57.13 ± 3.5
20	36.78 ± 2.7	18.32 ± 1.7	31.39 ± 2.2	NT[b]
21	12.86 ± 1.2	8.07 ± 0.6	15.86 ± 1.2	38.92 ± 2.8
22	10.23 ± 1.0	2.81 ± 0.2	7.28 ± 0.7	42.74 ± 3.0
Doxorubicin	4.50 ± 0.2	4.17 ± 0.2	5.23 ± 0.3	NT[b]

[a] IC_{50} values are the mean ± S.D. of three separate experiments. IC_{50} (μM): 1–10 (very strong); 11–20 (strong); 21–50 (moderate); 51–100 (weak); > 100 (non-cytotoxic).
[b] NT: Compounds not tested for their cytotoxicity against human normal cell (WI-38).
[c] NA: Compounds having IC_{50} value > 100 μM.

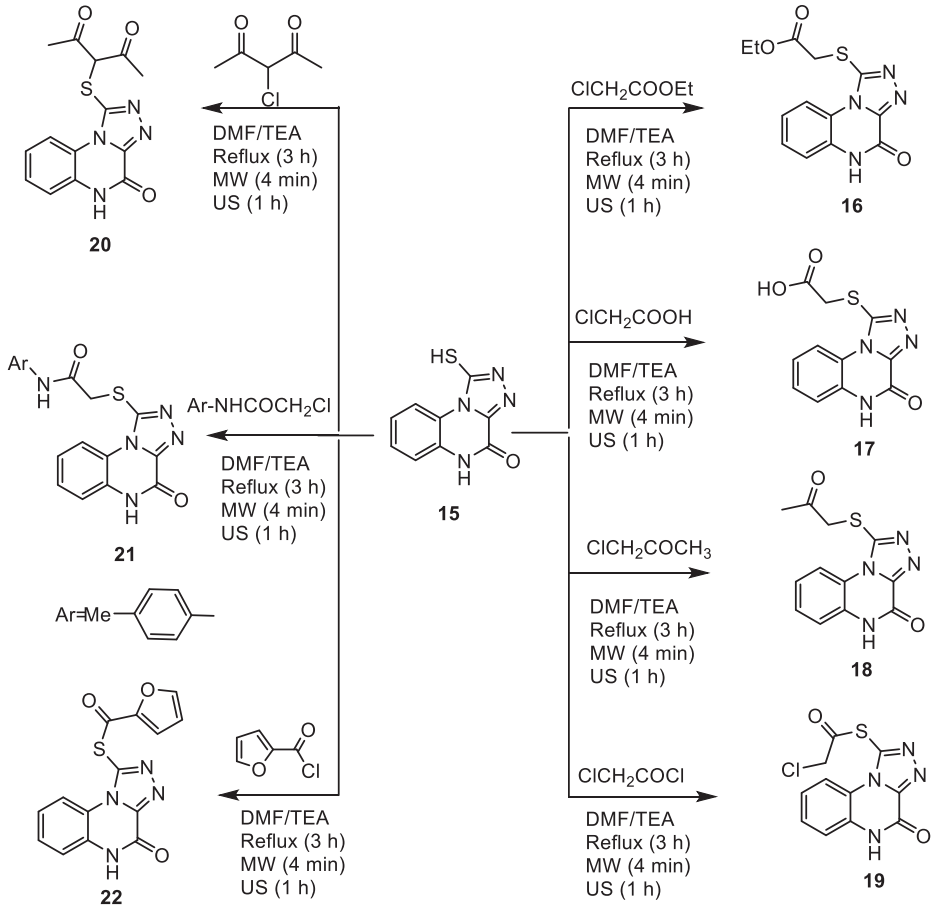

Scheme 3. Synthesis of the target compounds **16–22.**

Table 3
In vitro Topo II inhibitory activity and DNA intercalating affinity of the most active compounds.

Comp.	Topo II inhibition IC_{50} (μM)[a]	DNA intercalation IC_{50} (μM)[a]
12	0.89 ± 0.1	45.92 ± 2.4
15	1.06 ± 0.1	37.06 ± 1.9
19	0.62 ± 0.1	33.48 ± 1.8
21	0.45 ± 0.1	51.23 ± 2.7
22	0.52 ± 0.1	42.15 ± 2.1
Camptothecin	0.44 ± 0.1	NT[b]
Doxorubicin	NT[b]	31.22 ± 2.1

[a] IC_{50} values are the mean ± S.D. of three separate experiments
[b] NT: Compounds not tested

moderateIC_{50} values of 45.92, 51.23, and 42.15 μM, respectively.

2.2.5. Cell cycle analysis

In order to conserve tissue homeostasis, the balance between cell proliferation and death must be controlled. Through controlling a shared set of factors, some sort of regulation may be accomplished by coupling the process of cell cycle progression and programmed cell death. Accordingly, there is a link between the cell cycle and apoptosis arises from the accumulated evidence that manipulation of the cell cycle may either prevent or induce an apoptotic response [39–41].

In order to get an additional comprehension about the effect of compound **22** on the inhibition of cancer cell growth, its effect on cell cycle distribution and apoptosis induction was analyzed in HepG2 cells. In this work, HepG2 cell line was treated with compound **22** at a concentration 2.81 μM (the IC_{50} value of compound **22)** against untreated HepG2 cell for 24 h.

The results revealed that the percentage of HepG2 cells decreased at the G1 and S phases. For G1 phase, it decreased from 58.28% to 32.83%. At the S phase, it decreased from 27.11% to 13.68%. On the other hand, the percentage of HepG2 cells increased at G2/M and Sub-G1 phases. For G2/M phase, it increased from 12.83% to 51.33%. These results indicate that compound **22** could arrest the cell growth at G2/M phase (Table 4 and Fig. 4). Such findings were matched with the reported results which confirmed that the Topo II inhibitors can arrest the cell growth at G2/M phase [42].

2.2.6. Apoptosis analysis

Further investigation for apoptotic effect of compound **22** in HepG2 cells was carried out using Annexin V and PI double staining assay. In such procedure, HepG2 cells were treated with compound **22** at concentration of 2.81 μM, and allowed for incubation for 24 h.

Treatment of HepG2 cells with compound **22** resulted in an apoptotic effect by five time more than the untreated HepG2 cells. In details, compound **22** induced programmed cell death by 32.41% (early apoptosis = 32.23% & late apoptosis = 0.18%), compared to the control cells (6.35%) (Table 5 & Fig. 5).

2.2.7. Caspase-3 and caspase-9 determination

Caspases are crucial mediators of programmed cell death (apoptosis) [43–45]. Among them, caspase-3 is a frequently activated death protease, catalyzing the specific cleavage of many key cellular proteins [46]. Active caspase-9 works as an initiator for other caspases and then, activating downstream executioner caspases, initiating apoptosis [47]. Once activated, caspase-9 goes on to cleave caspase-3, -6, and -7, initiating the caspase cascade as they cleave several other cellular targets [48].

In order to examine the impact of compound **22** on the levels of both caspase-3 and caspase-9. HepG2 cells were treated with compound **22** at a concentration of 2.81 μM for 24 h. The results revealed that it produced a marked increase in the level of caspase-3 (405.21 pg/mL, 10 folds) compared to the control cells (40.76 pg/mL). In addition, the compound **22** exhibited a significant increase in the level of caspase-9 (35.71 ng/mL, 7 folds) compared to the control cells (4.86 ng/mL) (Table 6 & Fig. 6).

2.3. Docking studies

In this work, docking study was carried out for the designed compounds. Doxorubicin as a DNA intercalator was used as a reference ligand. The main aim of this study is to obtain additional comprehension about the binding modes of the designed compounds against the prospective target (DNA-topoisomerase II complex (PDB ID: 4G0U)). Table 7 illustrates the binding free energies (ΔG) of the docked compound**.** The reported key binding site of DNA-topoisomerase II complex involves Arg503, Asp479, Met782, Gln778, Ade12, Cyt8, Cyt11, Thy9, and Gua13 [49].

The binding mode of doxorubicin exhibited binding energy of −55.15 kcal/ mol. Fig. 7 illustrates the different binding interactions in the active site, where the planar aromatic system formed twelve pi-pi interactions with Cyt8 Thy9, Ade12, Gua13, and Ala521. Doxorubicin formed five hydrogen bonds with Gua13, Arg503 and Lys505, with the lengths of 1.9, 2.4, 2.0, 1.8, and 2.2, °A. The sugar moiety was oriented into the minor groove of DNA. The obtained data were is in accordance with the reported results [24].

The results of docking study revealed that the docked compound have similar binding mode of doxorubicin. The binding energies of the docked compounds is ranging from −29.41 to −51.78 kcal/mol (Table 7).

Compound **10** showed a binding energy of − 51.78 kcal/mol. The planar aromatic system (quinoxalin-2(1*H*)-one) formed twelve hydrophobic interactions with Gua13, Cyt8, Ade12, and Thy9. Moreover, the terminal 2-((1,3-diphenyl-1*H*-pyrazol-4-yl)methylene) hydrazine moiety was oriented at the minor groove of DNA, forming three hydrophobic interactions with Ala521and Ile454 (Fig. 8).

Compound **12** exhibited a binding energy of − 41.01 kcal/mol. The planar aromatic system (quinoxalin-2(1*H*)-one) formed nine pi-pi interactions with Ade12, Gua13, Cyt8 and Thy9. The 2-cyclohexylidenehydrazineside chain was oriented at the minor groove of DNA, forming one hydrophobic interaction with Ala521 (Fig. 9).

Compound **22** exhibited a binding energy of − 37.33 kcal/mol. The planar aromatic system (quinoxalin-2(1*H*)-one) formed fifteen pi-pi interactions with Ade12, Gua13, Cyt8 and Thy9. The furan-2-carbothioate side chain was oriented at the minor groove of DNA (Fig. 10). The binding mode of compound **15** and **19** were presented in Supplementary data.

Table 4
Effect of compound **22** on cell cycle progression in HepG2 cells after 24 h treatment.

Sample	Cell cycle distribution (%)[a]			
	%Sub-G1	%G1	%S	% G2/M
HepG2	1.77 ± 0.10	58.28 ± 2.38	27.11 ± 2.72	12.83 ± 1.25
Compound22 /HepG2	2.14 ± 0.21	32.83 ± 2.25**	13.68 ± 1.27*	51.33 ± 3.64***

[a] Values are given as mean ± SEM of three independent experiments. *p < 0.05, **p < 0.01, and ***p < 0.001 indicate statistically significant differences from the corresponding control (HepG2) group in unpaired *t*-tests.

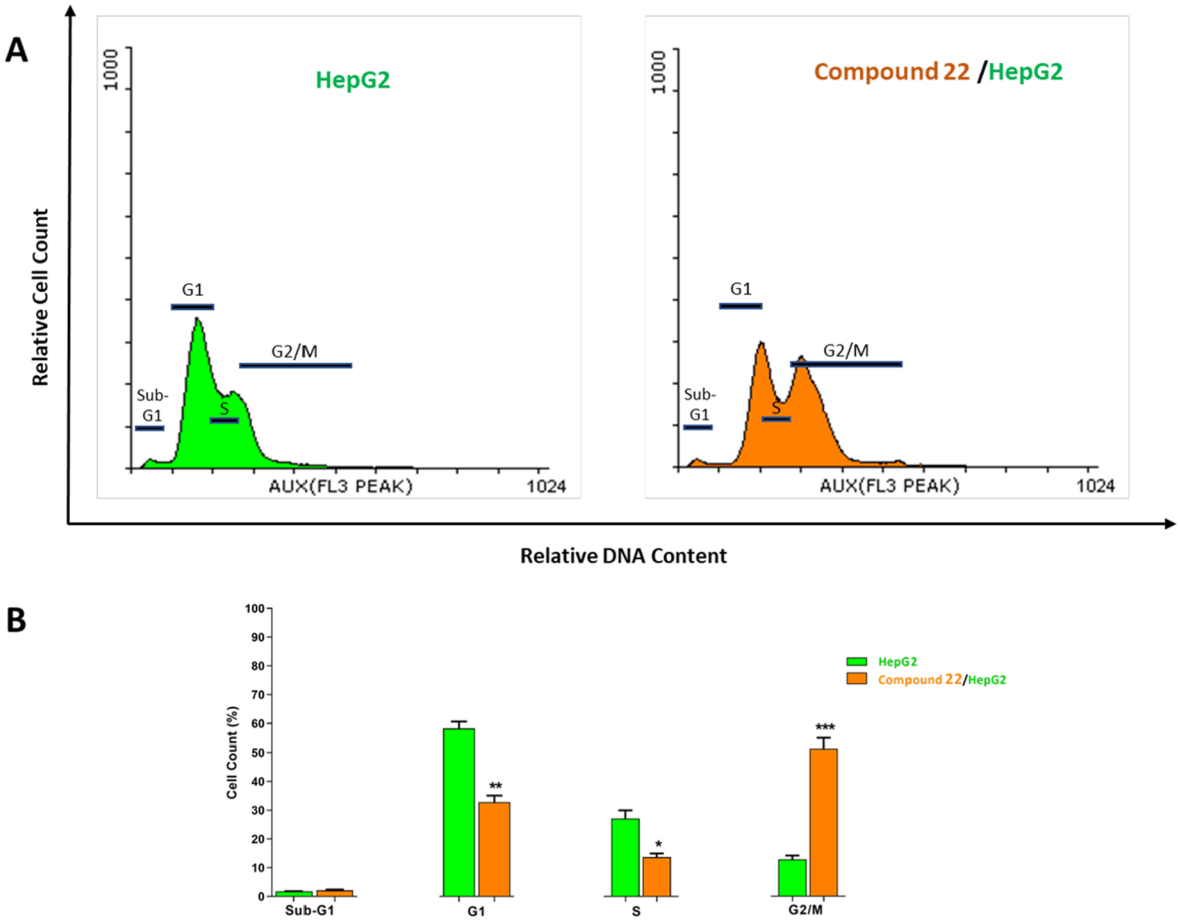

Fig. 4. Flow cytometric analysis of cell cycle phases post the compound **22** treatment. HepG2 Cells were treated with 2.81 μM (IC_{50} value) of compound **22** for 24 h. Then, the cells were harvested, stained with propidium iodide, and analyzed for cell distribution during the various phases of the cell cycle using Flowing software. (**A**) The representative histograms show the cell cycle distribution of control (HepG2), and cells treated with compound **22**. (**B**) Column graphs show the percentage of cells in each phase of the cell cycle. Values are given as mean ± SEM of three independent experiments. *p < 0.05, **p < 0.01, and ***p < 0.001 indicate statistically significant differences from the untreated control (HepG2) group in unpaired *t*-tests.

2.4. Structure-Activity Relationship (SAR)

In order to understand the trend of cytotoxic activities of the synthesized compounds against the tested cell lines, we correlated the different cytotoxicities to each other (Fig. 11). The blue line represents IC_{50} values against HCT-116, the green line represents the IC_{50} values against HepG2 cells, and red line represents IC_{50} values against MCF-7 cells. By investigation the three lines, it can be observed that the trends for all of them are similar for some extent. This indicated that the sensitivities of the tested cells are almost the same. So that, the SAR can be built on the total results of cytotoxicity.

In general, studying the cytotoxic activities of the synthesized compounds against HCT-116, HepG2, and MCF-7 cells, revealed that the derivatives of scaffold-1 consisted of three fused aromatic system ([1,2,4]triazolo[4,3-*a*]quinoxalin-4(5*H*)-one) were more active than that of scaffold-2 consisted of two fused aromatic system (quinoxalin-2(1*H*)-one).

With regard to scaffold-1, it was found that 1- mercapto derivative **15** was more active than 1-methyl derivative **14**, which was more active than the unsubstituted derivative **13**. Substitution on SH group of scaffold-1 produced less active derivatives except compound **19**. Then, we explored the impact of substitution on the thiol group of scaffold-1 by different moieties. It was found that aromatic substituted derivatives as compounds **21** and **22** more active than that with aliphatic substitution as compounds **16–20**. For aromatic derivatives, it was found that heterocyclic derivative **22** was more active than the non-hetero aromatic one **21**. With regard to aliphatic derivatives, it was found that the activities decreased in the order of chloroacetyl **19** > acetyl acetone **20** > acetone **18** > acetic acid **17** > ethyl acetate **16**.

For scsffold-2, we explored the activities of different hydrazone

Table 5
Effect of compound **22** on stages of the cell death process in HepG2 cells after 24 h treatment.

Sample	Viable[a] (Left Bottom)	Apoptosis[a]		Necrosis[a] (Left Top)
		Early (Right Bottom)	Late (Right Top)	
HepG2	93.54 ± 0.61	6.22 ± 0.61	0.13 ± 0.01	0.14 ± 0.01
Compound22 /HepG2	67.28 ± 3.48	32.23 ± 3.24**	0.18 ± 0.03	0.27 ± 0.11

[a] Values are given as mean ± SEM of three independent experiments. **p < 0.01 indicates statistically significant difference from the corresponding control (HepG2) group in unpaired *t*-tests.

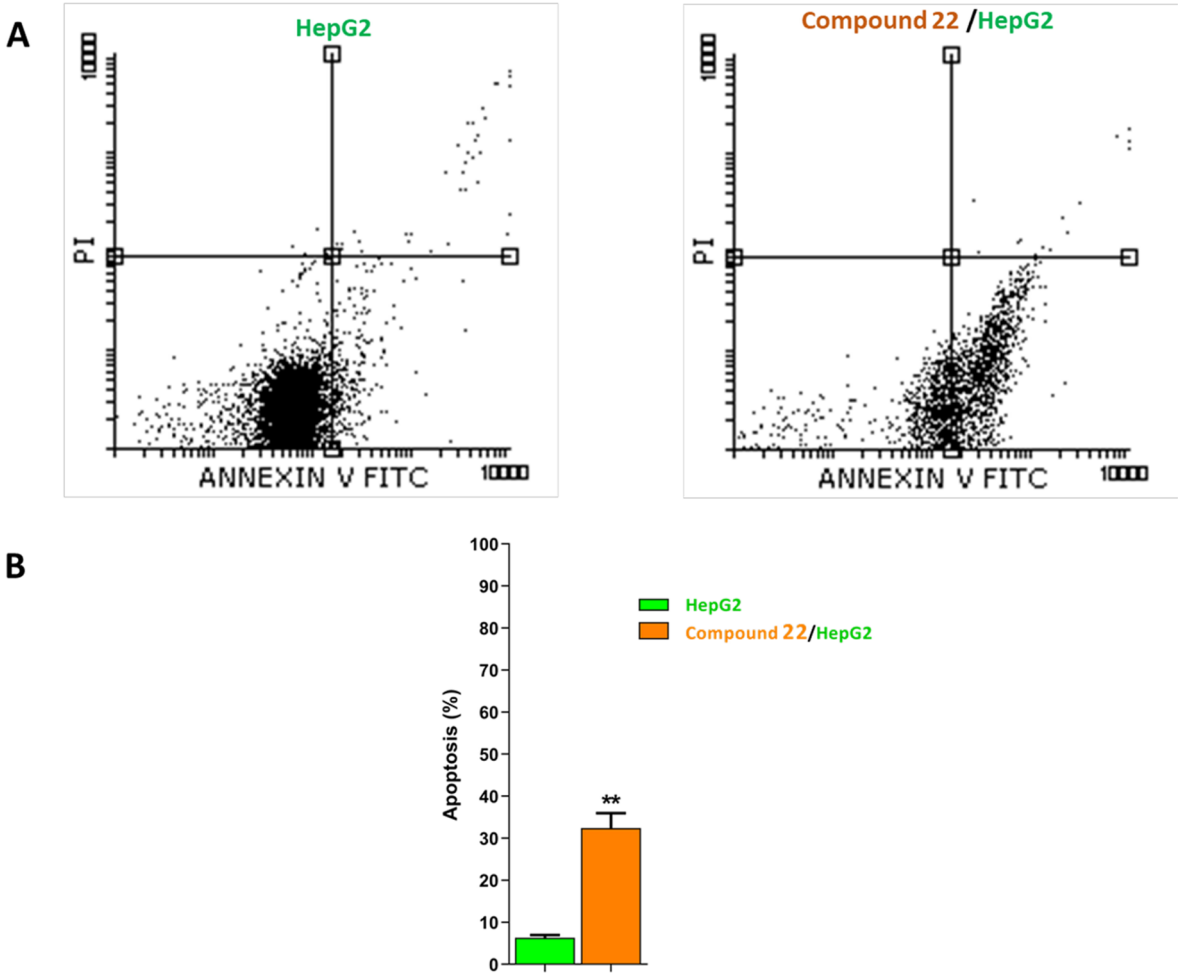

Fig. 5. Flow cytometric analysis of apoptosis in HepG2 cells exposed to compound **22**. HepG2 cells were treated with compound **22** (2.81 μM) for 24 h, harvested, stained with Annexin-V/propidium iodide (PI), and analyzed for apoptosis using Flowing Software. (**A**) The representative flow cytometric charts for control (HepG2) and the cells treated with compound **22**. For each dot plot chart, the quadrant regions represent the cells in each sub-population; lower left quadrant (Viable cells), lower right quadrant (Early apoptosis), upper right quadrant (Late apoptosis), and upper left quadrant (Necrosis). (**B**) Quantification of apoptosis from HepG2 cells treated with or without compound **22**. Values are given as mean ± SEM of three independent experiments. **$p < 0.01$ indicates statistically significant difference from the untreated control (HepG2) group in unpaired *t*-tests.

Table 6
Effect of compound **22** on active caspase-3 and caspase-9 in HepG2 cells after 24 h treatment.

Sample	Caspase-3 (pg/mL)[a]	Caspase-9 (ng/mL)[a]
HepG2	40.76 ± 1.74	4.86 ± 0.53
Compound22 /HepG2	405.21 ± 29.87 ***	35.71 ± 2.25 ***

[a] Values are given as mean ± SEM of three independent experiments. ***$p < 0.001$ indicates statistically significant difference from the corresponding control (HepG2) group in unpaired *t*-tests.

derivatives. It was found that the activities decreased in the order of cyclohexanone **12** > 2-acetylfuran **6** > 4-methylacetophenone **8** > 2-acetylthiophene **5** > 4-acetylbiphenyl **7** > 1-indanone **11** > 1,3-diphenyl-1*H*-pyrazole-4-carbaldehyde **10** > 6-chloro-4-oxo-4*H*-chromene-3-carbaldehyde **9**.

3. Conclusion

In summary, eighteen new quinoxaline derivatives were designed and eco-friendly synthesized. Three methods of synthesis were used including conventional, ultrasound irradiation and microwave-assisted. The structures of the new derivatives were confirmed via spectral and analytical analyses. The synthesized compounds were tested *in vitro* for their anti-proliferative effects against HCT-116, HepG2, and MCF-7 using MTT assay. Compounds **12**, **15**, **19**, **21**, and **22** exhibited good anti-proliferative activities against the tested cells with IC_{50} values ranging from 2.81 to 10.23 μM. Additional examinations were carried out for the most active members including toxicity test, Topo II inhibition, and DNA-binding assay. These compounds showed low toxicity against normal human cells (WI-38), good Topo II inhibitory activities with IC_{50} ranging from 0.45 to 1.06 μM, and DNA-binding affinities with IC_{50} ranging from 33.48 to 51.23 μM. Structure-activity relationship revealed that the derivatives of scaffold-1 consisted of three fused aromatic system ([1,2,4]triazolo[4,3-*a*]quinoxalin-4(5*H*)-one) were more active than that of scaffold-2 consisted of two fused aromatic system (quinoxalin-2(1*H*)-one). Moreover, compound **22** arrested the cell cycle of HepG2 cells at G2/M phase. The apoptotic effect of compound **22** (32.41%) was five times greater than that in control cells (6.35%). Additionally, compound **22** produced a significant increase in the level of caspase-3 (405.21 pg/mL, 10 folds) compared to the control cells (40.76 pg/mL), and caused an increase in the level of caspase-9 (35.71 ng/mL, 7 folds) compared to the control cells (4.86 ng/mL). The results of docking studies revealed that the docked compound have similar binding mode of doxorubicin with binding energies ranging from − 29.41 to − 46.03 kcal/mol.

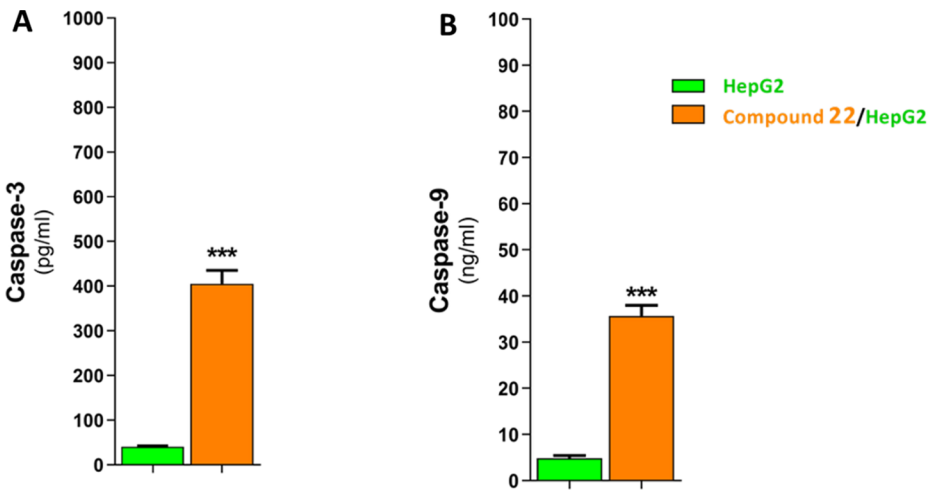

Fig. 6. Graphical representation for active caspase-3 and caspase-9 assay of compounds **22**. HepG2 cells were incubated with the compound **22** (2.81 μM) for 24 h. Cells were then collected for the quantification of caspase-3 (**A**) and caspase-9 (**B**). The data are present as the mean ± S.E.M. from three independent experiments. ***$p < 0.001$ indicates statistically significant difference from the corresponding control (HepG2) group in unpaired *t*-tests.

Table 7
The docking binding free energies (**ΔG**) of the synthesized compounds with DNA-topoisomerase II complex.

Comp.	ΔG (kcal/mol)	Comp.	ΔG (kcal/mol)
5	−39.44	**15**	−30.69
6	−42.21	**16**	−46.03
7	−46.50	**17**	−33.07
8	−42.51	**18**	−41.38
9	−44.81	**19**	−39.86
10	−51.78	**20**	−44.85
11	−42.55	**21**	−49.71
12	−41.01	**22**	−37.33
13	−29.41	**Doxorubicin**	− 55.15
14	−31.96		

4. Experimental

4.1. Chemistry

4.1.1. General

All melting points were measured on a Gallen Kamp melting point apparatus (Sanyo Gallen Kamp, UK) and were uncorrected. The Microwave reactions were done by Microsynth instrument type MA143 (Micro wave flux). The ultrasound-assisted reactions were performed in Digital Ultrasonic Cleaner CD-4830 (35 KHz, 310 W). The IR spectra were recorded on a Pye-Unicam SP-3–300 infrared spectrophotometer and expressed in wave number (cm^{-1}). ^{1}H NMR spectra were run at 400 MHz, Bruker Avance III NMR spectrometer. TMS was used as an internal standard in deuterated dimethylsulphoxide (DMSO-d_6). Chemical shifts (δ) are quoted in ppm. All coupling constant (*J*) values are given in hertz. Elemental analyses were performed on CHN analyzer and all compounds were within ± 0.4 of the theoretical values. The reactions were monitored by thin-layer chromatography (TLC) using TLC sheets coated with UV fluorescent silica gel Merck 60 F254 plates and were visualized using UV lamp and different solvents as mobile phases. All reagents and solvents were purified and dried by standard techniques. Compound **3, 4**, and **12** were synthesized according to the reported procedures [50,51].

4.1.2. General procedure for synthesis of compounds *5–12*

a. **Conventional Method**

A mixture of compound **4** (10 mmol, 1.76 g) and carbonyl derivatives (10 mmol) namely, 2-acetylthiophene, 2-Acetylfuran, 4-acetylbiphenyl, 4-methylacetophenone, 6-chloro-4-oxo-4*H*-chromene-3-carbaldehyde, 1,3-diphenyl-1*H*-pyrazole-4-carbaldehyde, 1-indanone, and cyclohexanone was refluxed for 4 h in ethanol (20 mL). The formed

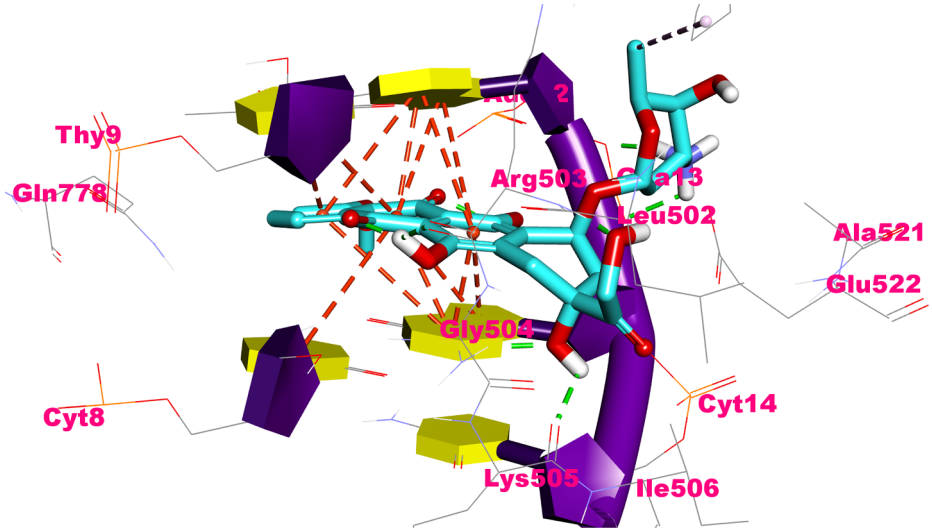

Fig. 7. Binding of doxorubicin with DNA-Topo II complex, the hydrogen bonds are represented in green dashed lines and the pi interactions are represented in orange dashed lines. (For interpretation of the references to color in this figure legend, the reader is referred to the web version of this article.)

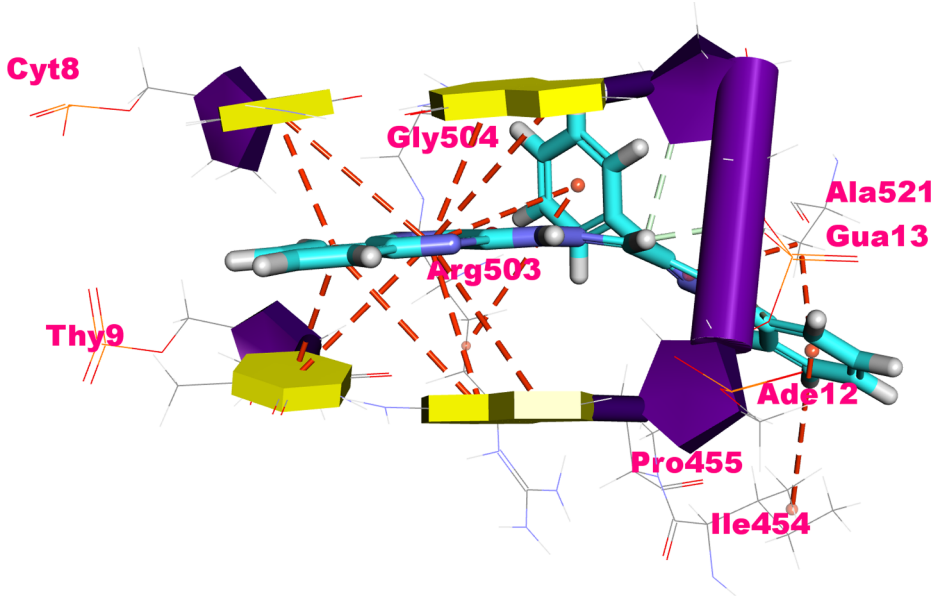

Fig. 8. Binding of compound **10** with DNA-Topo II complex, the hydrogen bonds are represented in green dashed lines and the pi interactions are represented in orange dashed lines. (For interpretation of the references to color in this figure legend, the reader is referred to the web version of this article.)

precipitate was filtered, washed several times with ethanol, dried and crystallized to give the target compounds **5–12,** respectively.

b. **Under Microwave method**

A mixture of **4** (10 mmol, 1.76 g) and carbonyl derivatives (10 mmol) namely, 2-2-acetylthiophene, 2-Acetylfuran, 4-acetylbiphenyl, 4-methylacetophenone, 6-chloro-4-oxo-4*H*-chromene-3-carbaldehyde, 1,3-diphenyl-1H-pyrazole-4-carbaldehyde, 1-indanone, and cyclohexanone, in ethanol (20 mL) was added to the reaction vessel placed into the microwave reactor. The mixture was allowed to react under microwave irradiation of 200–400 W at 120 °C for 30 min. with continuous stirring via the automatic mode. The reaction was monitored using TLC. After completion of the reaction and cooling, the product was obtained and crystallized from the proper solvent to give the corresponding final compounds **5–12,** respectively.

4.1.2.1. 3-(2-(1-(Thiophen-2-yl)ethylidene)hydrazineyl)quinoxalin-2(1H)-one ***5***. Brown crystals; m.p. 300 < °C; IR (KBr, cm^{-1}): 3316 (NH), 3062 (CH aromatic), 2889 (CH aliphatic), 1698 (CO); ^{1}H NMR (400 MHz, DMSO-d_6) δ (ppm): 2.40 (s, 3H, CH_3, for *Z* isomer), 2.41 (s, 3H, CH_3, for *E* isomer) 6.91–7.66 (m, 14H, Ar-H), 9.61 (s, 1H, NH, D_2O exchangeable, for *E* isomer), 9.92 (s, 1H, NH, D_2O exchangeable, for *Z* isomer), 11.54 (s, 1H, NH, D_2O exchangeable, for *E* isomer), 12.47 (s, 1H, NH, D_2O exchangeable, for Z isomer); Anal. Calcd for: $C_{14}H_{12}N_4OS$ (284.34): C, 59.14; H, 4.25; N, 19.70; Found: C, 58.92; H, 4.18; N, 19.61%.

4.1.2.2. 3-(2-(1-(Furan-2-yl) ethylidene)hydrazineyl)quinoxalin-2(1H)-one ***6***. Yellow crystals; m.p. 300 < °C; IR (KBr, cm^{-1}): 3339 (NH), 3063 (CH aromatic), 2845 (CH aliphatic), 1682 (CO); ^{1}H NMR (400 MHz, DMSO-d_6) δ (ppm): 2.30 (s, 3H, CH_3, for *Z* isomer), 2.31 (s, 3H, CH_3, for *E* isomer), 6.61–8.09 (m, 14H, Ar-H), 9.55 (s, 1H, NH, D_2O exchangeable, for *E* isomer), 10.11 (s, 1H, NH, D_2O exchangeable, for *Z* isomer), 11.55 (s, 1H, NH, D_2O exchangeable, for *E* isomer), 12.49 (s, 1H, NH, D_2O exchangeable, for Z isomer); Anal. Calcd for:

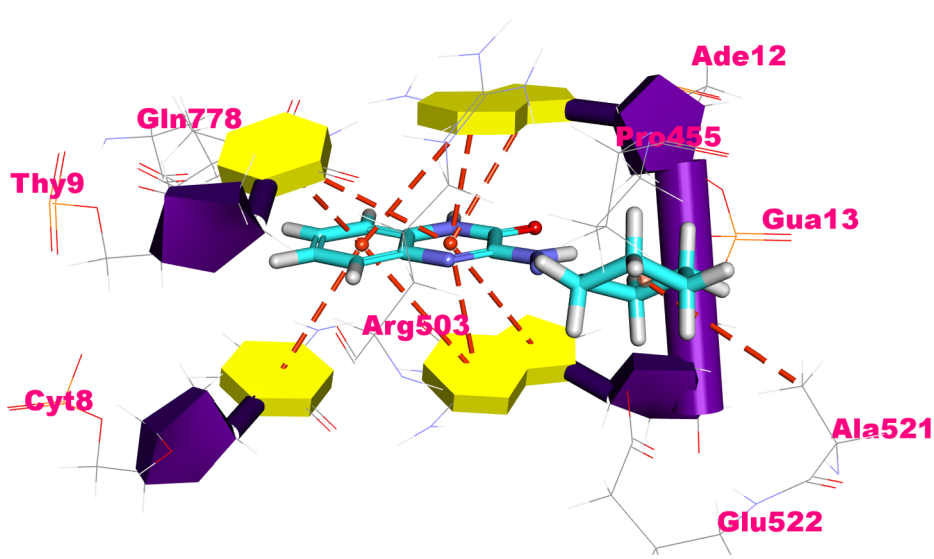

Fig. 9. Binding of compound **12** with DNA-Topo II complex, the hydrogen bonds are represented in green dashed lines and the pi interactions are represented in orange dashed lines. (For interpretation of the references to color in this figure legend, the reader is referred to the web version of this article.)

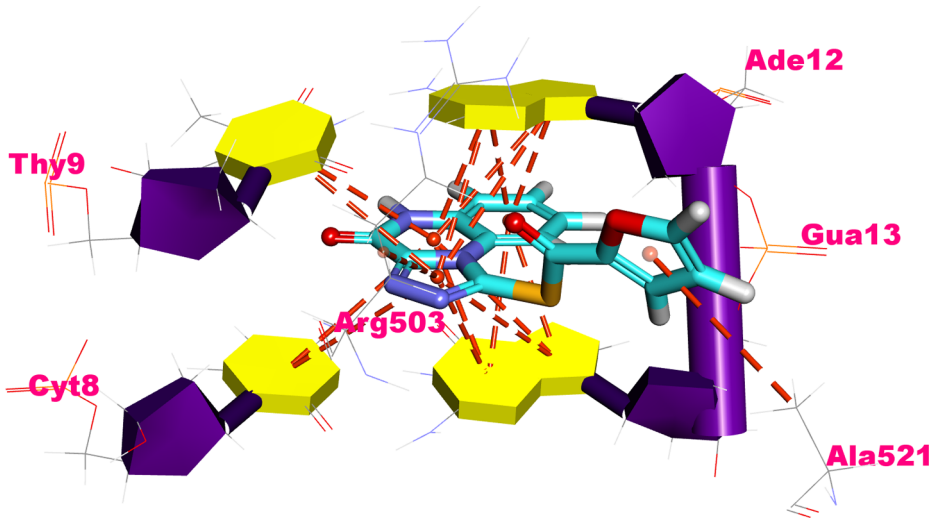

Fig. 10. Binding of compound **22** with DNA-Topo II complex, the hydrogen bonds are represented in green dashed lines and the pi interactions are represented in orange dashed lines. (For interpretation of the references to color in this figure legend, the reader is referred to the web version of this article.)

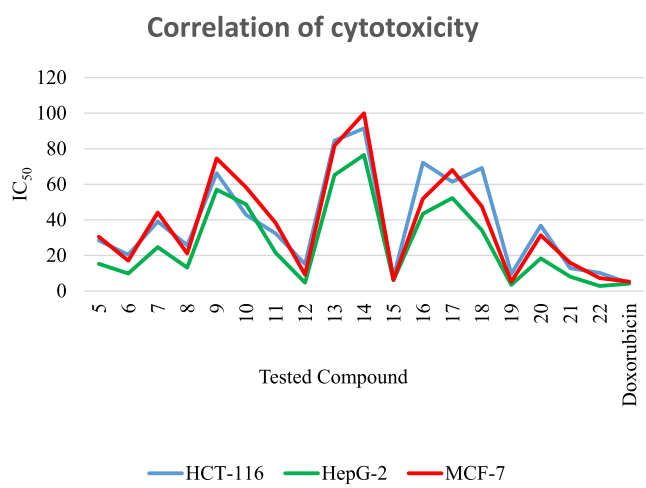

Fig. 11. Correlation of cytotoxic activities of the synthesized compounds against HCT-116, HepG2, and MCF-7 cells.

$C_{14}H_{12}N_4O_2$ (268.28): C, 62.68; H, 4.51; N, 20.88; Found: C, 62.51; H, 4.44; N, 20.79%.

*4.1.2.3. 3-(2-(1-((1,1′-Biphenyl)-4-yl)ethylidene)hydrazineyl)quinoxalin-2(1H)-one **7**.* Buff crystals; m.p. 300 < °C; IR (KBr, cm^{-1}): 3343 (NH), 3032 (CH aromatic), 2848 (CH aliphatic), 1663 (CO); ^{1}H NMR (400 MHz, DMSO-d_6) δ (ppm): 2.31 (s, 3H, CH_3, for *Z* isomer), 2.32 (s, 3H, CH_3, for *E* isomer), 6.94–8.16 (m, 26H, Ar-H), 9.66 (s, 1H, NH, D_2O exchangeable, for *Z* isomer), 10.20 (s, 1H, NH, D_2O exchangeable, for *E* isomer), 11.55 (s, 1H, NH, D_2O exchangeable, for *E* isomer), 12.51 (s, 1H, NH, D_2O exchangeable, for *Z* isomer); Anal. Calcd for: $C_{22}H_{18}N_4O$ (354.15): C, 74.56; H, 5.12; N, 15.81; Found: C, 74.29; H, 5.03; N, 15.63%.

*4.1.2.4. 3-(2-(1-(p-Tolyl)ethylidene)hydrazineyl)quinoxalin-2(1H)-one **8**.* Yellow crystals; m.p. 222–224 °C; IR (KBr, cm^{-1}): 3353 (NH), 3037 (CH aromatic), 2846 (CH aliphatic), 1668 (CO); ^{1}H NMR (400 MHz, DMSO-d_6) δ (ppm): 2.31 (s, 3H, CH_3 CH_3, for *Z* isomer), 2.35 (s, 3H, CH_3, for *E* isomer), 2.38 (s, 3H, CH_3, for *Z* isomer), 2.41 (s, 3H, CH_3, for *E* isomer), 6.90–7.98 (m, 16H, Ar-H), 9.59 (s, 1H, NH, D_2O exchangeable, for *Z* isomer), 11.53 (s, 1H, NH, D_2O exchangeable, for *E* isomer), 12.48 (s, 1H, NH, D_2O exchangeable, for *E* isomer), 11.53 (s, 1H, NH, D_2O exchangeable, for *Z* isomer); Anal. Calcd for: $C_{17}H_{16}N_4O$ (292.34): C, 69.85; H, 5.52; N, 19.17; Found: C, 69.72; H, 5.47; N, 19.02%.

*4.1.2.5. 3-(2-((6-Chloro-4-oxo-4H-chromen-3-yl) methylene)hydrazineyl) quinoxalin-2(1H)-one **9**.* Yellow crystals; m.p 280–283 °C; IR (KBr, cm^{-1}): 3160 (NH), 3049 (CH aromatic), 1684 (CO); ^{1}H NMR (400 MHz, DMSO-d_6) δ (ppm): 7.01 (d, 1H, Ar-H, J = 7.6), 7.35 (dd, 1H, Ar-H), 7.44 (s, 1H, Ar-H), 7.46 (dd, 1H, Ar-H), 7.56 (d, 1H, Ar-H, J = 8.4), 7.59 (d, 1H, Ar-H, J = 8.4), 7.79 (d, 1H, Ar-H, J = 8), 8.22 (s, 1H, Ar-H), 9.26 (s, 1H, olefinic H), 10.58 (s, 1H, NH, D_2O exchangeable), 13.02 (s, 1H, NH, D_2O exchangeable); Anal. Calcd for: $C_{18}H_{11}ClN_4O_3$ (366.76): C, 58.95; H, 3.02; N, 15.28; Found: C, 58.82; H, 2.94; N, 15.15%.

*4.1.2.6. 3-(2-((1,3-Diphenyl-1H-pyrazol-4-yl)methylene)hydrazineyl) quinoxalin-2(1H)-one **10**.* Orange crystals; m.p. 300 < °C; IR (KBr, cm^{-1}): 3179 (NH), 3056 (CH aromatic), 1695 (CO); ^{1}H NMR (400 MHz, DMSO-d_6) δ (ppm): 7.05 (d, 1H, Ar-H, J = 8 Hz), 7.20 (d, 2H, Ar-H, J = 8), 7.34 (dd, 1H, Ar-H), 7.44 (dd, 1H, Ar-H), 7.44 (dd, 1H, Ar-H), 7.53 (d, 2H, Ar-H, J = 8), 7.54 (dd, 1H, Ar-H), 7.65 (d, 2H, Ar-H, J = 8), 7.76 (d, 2H, Ar-H, J = 8), 7.81 (d, 1H, Ar-H, J = 8), 8.76 (s, 1H, Ar-H, CH of pyrazole), 8.99 (s, 1H, olefinic H), 9.57 (s, 1H, NH, D_2O exchangeable), 11.25 (s, 1H, NH, D_2O exchangeable); Anal. Calcd for: $C_{24}H_{18}N_6O$ (406.15): C, 70.92; H, 4.46; N, 20.68; Found: C, 70.79; H, 4.37; N, 20.55%.

*4.1.2.7. 3-(2-(2,3-Dihydro-1H-inden-1-ylidene)hydrazineyl)quinoxalin-2(1H)-one **11**.* Brown crystals; m.p. 292–294 °C; IR (KBr, cm^{-1}): 3339 (NH), 3046 (CH aromatic), 1690 (CO); ^{1}H NMR (400 MHz, DMSO-d_6) δ (ppm): 2.98 (t, 2H, CH_2), 3.05 (t, 2H, CH_2), 6.93 (d, 1H, Ar-H, J = 8), 7.11 (dd, 1H, Ar-H), 7.19 (dd, 1H, Ar-H), 7.33 (dd, 1H, Ar-H), 7.35 (dd, 1H, Ar-H), 7.51 (d, 1H, Ar-H, J = 7.4), 7.75 (d, 1H, Ar-H, J = 7.6), 8.08 (d, 1H, Ar-H, J = 7.2), 9.34 (s, 1H, NH, D_2O exchangeable), 11.53 (s, 1H, NH, D_2O exchangeable); Anal. Calcd for: $C_{17}H_{14}N_4O$ (290.33): C, 70.33; H, 4.86; N, 19.30; Found: C, 70.20; H, 4.78; N, 19.18%.

*4.1.3. General procedure for synthesis of compounds **13** and **14***

a. **Conventional Method**

A mixture of **4** (10 mmol, 1.76 g) and carboxylic acid derivatives (10 mmol) namely, formic acid and acetic acid was refluxed for 1 h. The formed precipitate was filtered, dried and crystallized from ethanol to

afford the corresponding compounds **13** and **14**, respectively.

b. **Under Microwave method**

A mixture of **4** (10 mmol, 1.76 g) and carboxylic acid derivatives (10 mL) namely, formic acid and acetic acid was added to the reaction vessel placed into the microwave reactor. The mixture was allowed to react under microwave irradiation of 200–400 W at 120 °C for 3 min. with continuous stirring via the automatic mode. The reaction was monitored using TLC. After completion of the reaction and cooling, the product was obtained and crystallized from the proper solvent to give the corresponding target compounds **13** and **14**, respectively.

c. **Under Sonication method**

A mixture of **4** (10 mmol, 1.76 g) and carboxylic acid derivatives (10 mL) namely, formic acid and acetic acid, was placed in Erlenmyer flask (50 mL) and subjected to ultrasound waves at room temperature for 30 min. The formed precipitate was filtered, dried, and crystallized from the appropriate solvent to afford the target compounds **13** and **14**, respectively.

*4.1.3.1. [1,2,4] Triazolo[4,3-a]quinoxalin-4(5H)-one **13***. Yellow crystals; m.p. 300 < °C; IR (KBr, cm^{-1}): 3105 (NH), 3010 (CH aromatic), 1693 (CO); ^{1}H NMR (400 MHz, DMSO-d_6) δ (ppm): 7.29 (dd, 1H, Ar-H, H-8 of quinoxaline), 7.37 (d, 1H, Ar-H, J = 8, H-7 of quinoxaline), 7.42 (dd, 1H, Ar-H, H-6 of quinoxaline), 8.14 (d, 1H, Ar-H, J = 8.2, H-9 of quinoxaline), 9.86 (s, 1H, Ar-H, *N*-CH = N), 12.01 (s, 1H, NH, D_2O exchangeable); Anal. Calcd for: $C_9H_6N_4O$ (186.17): C, 58.06; H, 3.25; N, 30.09; Found: C, 57.90; H, 3.18; N, 29.05%.

*4.1.3.2. 1-Methyl-[1,2,4]triazolo[4,3-a]quinoxalin-4(5H)-one **14***. Orange crystals; m.p. 300 < °C; IR (KBr, cm^{-1}): 3145 (NH), 3035 (CH aromatic), 2855 (CH aliphatic) 1673 (CO); ^{1}H NMR (400 MHz, DMSO-d_6) δ (ppm): 2.97 (s, 3H, CH_3), 6.94 (dd, 1H, Ar-H, H-8 of quinoxaline), 7.30 (dd, 1H, Ar-H, H-7 of quinoxaline), 7.43 (d, 1H, Ar-H, J = 8 Hz, H-6 of quinoxaline), 8.04 (d, 1H, Ar-H, J = 8 Hz, H-9 of quinoxaline), 11.98 (s, 1H, NH, D_2O exchangeable); Anal. Calcd for: $C_{10}H_8N_4O$ (200.20): C, 59.99; H, 4.03; N, 27.99; Found: C, 59.85; H, 3.94; N, 27.87%.

*4.1.4. General procedure for synthesis of compound **15***

a. **Conventional Method**

Method (a)

A mixture of **4** (10 mmol, 1.76 g) and CS_2 (10 mmol, 0.76 mL, 0.76 g) in pyridine (20 mL) was refluxed for 4 h. The reaction mixture was poured on to ice water and acidified using dil. HCl. The formed precipitate was filtered, washed several times with water, dried and crystallized to give compound **15**.

Method (b)

A mixture of **4** (10 mmol, 1.76 g), CS_2 (10 mmol, 0.76 mL, 0.76 g) and potassium hydroxide (10 mmol, 0.56 g), was refluxed in absolute ethanol (20 mL) for 5 h. The mixture was cooled to room temperature and poured onto 1 N HCl (20 mL). The yellow precipitated product was filtered, washed with water, filtered, dried, and crystallized from ethanol to afford compound **15**.

b. **Under Sonication method**

A mixture of **4** (10 mmol, 1.76 g), CS_2 (10 mmol, 0.76 mL, 0.76 g) and potassium hydroxide (10 mmol, 0.56 g) in absolute ethanol (20 mL) was placed in Erlenmyer flask (50 mL) and subjected to ultrasound waves at room temperature for 60 min. The yellow precipitated product was filtered, washed with water, dried and crystallized from ethanol to afford compound **15**.

*4.1.4.1. 1-Mercapto-[1,2,4]triazolo[4,3-a]quinoxalin-4(5H)-one **15***. Yellow crystals; m.p. 300 < °C; IR (KBr, cm^{-1}): 3373 (NH), 3073 (CH aromatic), 1700 (CO).^{1}H NMR (400 MHz, DMSO-d_6) δ (ppm): 7.22 (dd, 1H, Ar-H, H-8 of quinoxaline), 7.28 (d, 1H, Ar-H, J = 8 Hz, H-7 of quinoxaline), 7.36 (dd, 1H, Ar-H, H-6 of quinoxaline), 10.09 (d, 1H, Ar-H, J = 7.6 Hz, H-9 of quinoxaline), 12.00 (s, 1H, NH, D_2O exchangeable), 14.63 (s, 1H, SH, D_2O exchangeable); Anal. Calcd for: $C_9H_6N_4OS$ (218.23): C, 49.53; H, 2.77; N, 25.67; Found: C, 49.42; H, 2.69; N, 25.54%.

*4.1.5. General procedure for synthesis of compounds **16–22***

a. **Conventional Method**

A mixture of **15** (10 mmol, 2.18 g) and different halide derivatives (10 mmol) namely, ethyl chloroacetate, chloroacetic acid, chloroacetone, chloroacetyl chloride, 2-chloro-*N*-(*p*-tolyl) acetamide, and furoyl chloride was refluxed in DMF (20 mL) for 3 h in the presence of few drops of piperidine. The mixture was cooled and the formed solid products were filtered, dried and crystallized from ethanol to afford the corresponding compounds **16–22** respectively.

b. **Under Microwave method**

A mixture of **15** (10 mmol, 2.18 g) and different halide derivatives (10 mmol) namely, ethyl chloroacetate, chloroacetic acid, chloroacetone, chloroacetyl chloride, 2-chloro-*N*-(*p*-tolyl) acetamide, and furoyl chloride, in DMF (20 mL) and few drops of piperidine was added to the reaction vessel placed into the microwave reactor. The mixture was allowed to react under microwave irradiation of 200–400 W at 120 °C for 4 min. with continuous stirring via the automatic mode. After completion of the reaction and cooling, the products were obtained and crystallized from the proper solvent to give the corresponding final compounds **16–22**, respectively.

c. **Under Sonication method**

A mixture of **15** (10 mmol, 2.18 g) and different halide derivatives (10 mmol) namely, ethyl chloroacetate, chloroacetic acid, chloroacetone, chloroacetyl chloride, 2-chloro-*N*-(*p*-tolyl) acetamide, and furoyl chloride, in DMF (20 mL) and few drops of piperidine was placed in Erlenmyer flask (50 mL) and subjected to ultrasound waves at room temperature for 60 min. The formed precipitates were filtered, dried, and crystallized from the appropriate solvent to afford the target compounds **16–22**, respectively.

*4.1.5.1. Ethyl 2-((4-oxo-4,5-dihydro-[1,2,4]triazolo[4,3-a]quinoxalin-1-yl)thio)acetate **16***. Yellow crystals; m.p.250–252 °C; IR (KBr, cm^{-1}): 3194 (NH), 3032 (CH aromatic), 2869 (CH aliphatic), 1733 (CO) and 1690 (CO); ^{1}H NMR (400 MHz, DMSO-d_6) δ (ppm): 1.15 (t, 3H, CH_3), 4.08 (q, 2H, CH_2 CH_3), 4.38 (s, 2H, CH_2-S), 7.25 (dd, 1H, Ar-H, H-8 of quinoxaline), 7.31 (dd, 1H, Ar-H, H-7 of quinoxaline), 7.45 (d, 1H, Ar-H, J = 8 Hz, H-6 of quinoxaline), 8.25 (d, 1H, Ar-H, J = 8 Hz, H-9 of quinoxaline), 12.00 (s, 1H, NH, D_2O exchangeable); Anal. Calcd for: $C_{13}H_{12}N_4O_3S$ (304.32): C, 51.31; H, 3.97; N, 18.41; Found: C, 51.17; H, 3.89; N, 18.27%.

*4.1.5.2. 2-((4-Oxo-4,5-dihydro-[1,2,4]triazolo[4,3-a]quinoxalin-1-yl) thio)acetic acid **17***. Pale yellow crystals; m.p.216–218 °C; IR (KBr, cm^{-1}): 3438 (OH), 3137 (NH), 3030 (CH aromatic), 2847 (CH aliphatic), 1694 (CO); ^{1}H NMR (400 MHz, DMSO-d_6) δ (ppm): 4.1 (s, 2H, CH_2), 7.32–7.46 (m, 3H, Ar-H), 8.33 (d, 1H, Ar-H, J = 8), 11.97 (s, 1H, NH, D_2O exchangeable); Anal. Calcd for: $C_{11}H_8N_4O_3S$ (276.27): C, 47.82; H, 2.92; N, 20.28; Found: C, 47.68; H, 2.87; N, 20.13%.

*4.1.5.3. 1-((2-Oxopropyl)thio)-[1,2,4]triazolo[4,3-a]quinoxalin-4(5H)-one **18***. White crystals; m.p.280–282 °C; IR (KBr, cm^{-1}: 3215 (NH), 3057 (CH aromatic), 2858 (CH aliphatic), 1711 (CO), 1692 (CO); ^1H NMR (400 MHz, DMSO-d_6) δ (ppm): 2.30 (s, 3H, CH_3), 4.56 (s, 2H, CH_2), 7.36 (dd, 1H, Ar-H, H-8 of quinoxaline), 7.40 (dd, 1H, Ar-H, H-7 of quinoxaline), 7.44 (d, 1H, Ar-H, J = 8 Hz, H-6 of quinoxaline), 8.25 (d, 1H, Ar-H, J = 8 Hz, H-9 of quinoxaline), 12.03 (s, 1H, NH, D_2O exchangeable); Anal. Calcd for: $C_{12}H_{10}N_4O_2S$ (274.30): C, 52.55; H, 3.67; N, 20.43; Found: C, 52.42; H, 3.61; N, 20.31%.

*4.1.5.4. 4-Oxo-4,5-dihydro-[1,2,4]triazolo[4,3-a]quinoxalin-1-yl-2-chloroethanethioate **19***. Pale yellow crystals; m.p.272–274 °C; IR (KBr, cm^{-1}): 3384 (NH), 3016 (CH aromatic), 2850 (CH aliphatic), 1688 (CO), 1671 (CO); ^1H NMR (400 MHz, DMSO-d_6) δ (ppm): 4.32 (s, 2H, CH_2), 7.22 (dd, 1H, Ar-H, H-8 of quinoxaline), 7.33 (dd, 1H, Ar-H, H-7 of quinoxaline), 7.40 (d, 1H, Ar-H, J = 8 Hz, H-6 of quinoxaline), 8.22 (d, 1H, Ar-H, J = 8 Hz, H-9 of quinoxaline), 12.01 (s, 1H, NH, D_2O exchangeable); Anal. Calcd for: $C_{11}H_7ClN_4O_2S$ (294.71): C, 44.83; H, 2.39; N, 19.01; Found: C, 44.69; H, 2.31; N, 19.11%.

*4.1.5.5. 3-((4-Oxo-4,5-dihydro-[1,2,4]triazolo[4,3-a]quinoxalin-1-yl) thio)pentane-2,4-dione **20***. Buff crystals; m.p.260–262 °C; IR (KBr, cm^{-1}): 3189 (NH), 3052 (CH aromatic), 2875 (CH aliphatic), 1685 (CO), 1677 (CO); ^1H NMR (400 MHz, DMSO-d_6) δ (ppm): 2.37 (s, 6H, $2CH_3$), 4.56 (s, 1H, CH), 7.34 (dd, 1H, Ar-H, H-8 of quinoxaline), 7.37 (dd, 1H, Ar-H, H-7 of quinoxaline), 7.45 (d, 1H, Ar-H, J = 8 Hz, H-6 of quinoxaline), 8.25 (d, 1H, Ar-H, J = 8 Hz, H-9 of quinoxaline), 12.03 (s, 1H, NH, D_2O exchangeable); Anal. Calcd for: $C_{14}H_{12}N_4O_3S$ (316.34): C, 53.16; H, 3.82; N, 17.71; Found: C, 53.02; H, 3.76; N, 17.61%.

*4.1.5.6. 2- ((4-Oxo-4,5-dihydro-[1,2,4]triazolo[4,3-a]quinoxalin-1-yl) thio)-N-(p-tolyl) acetamide **21***. Yellow crystals; m.p.292–294 °C; IR (KBr, cm^{-1}): 3195 (NH), 3057 (CH aromatic), 2870 (CH aliphatic), 1689 (CO), 1674 (CO), ^1H NMR (400 MHz, DMSO-d_6) δ (ppm): 2.23 (s, 3H, CH_3), 4.45 (s, 2H, CH_2), 7.09 (d, 2H, Ar-H, H-3 and H-5 of phenyl), 7.24 (d, 2H, Ar-H, H-2 and H-6 of phenyl), 7.28 (dd, 1H, Ar-H, H-8 of quinoxaline), 7.37 (dd, 1H, Ar-H, H-7 of quinoxaline), 7.45 (d, 1H, Ar-H, J = 8 Hz, H-6 of quinoxaline), 8.34 (d, 1H, Ar-H, J = 8 Hz, H-9 of quinoxaline), 12.01 (s, 1H, NH, D_2O exchangeable), 12.05 (s, 1H, NH, D_2O exchangeable); Anal. Calcd for: $C_{18}H_{15}N_5O_2S$ (365.41): C, 59.17; H, 4.14; N, 19.17; Found: C, 59.08; H, 4.07; N, 19.02%.

*4.1.5.7. 4-Oxo-4,5-dihydro-[1,2,4]triazolo[4,3-a]quinoxalin-1-yl-furan-2-carbothioate **22***. Buff crystals; m.p.288–290 °C; IR (KBr, cm^{-1}): 3120 (NH), 3040 (CH aromatic), 2878 (CH aliphatic), 1698 (CO), 1688 (CO); ^1H NMR (400 MHz, DMSO-d_6) δ (ppm): 7.23 (dd, 1H, Ar-H, H-4 of furan), 7.25 (d, 1H, Ar-H, H-3 of furan), 7.27 (dd, 1H, Ar-H, H-8 of quinoxaline), 7.31 (dd, 1H, Ar-H, H-7 of quinoxaline), 7.40 (d, 1H, Ar-H, J = 8 Hz, H-6 of quinoxaline), 8.43 (d, 1H, Ar-H, J = 8 Hz, H-9 of quinoxaline), 8.36 (d, 1H, Ar-H, J = 8, H-5 of furan), 12.01 (s, 1H, NH, D_2O exchangeable); Anal. Calcd for: $C_{14}H_8N_4O_3S$ (312.30): C, 53.84; H, 2.58; N, 17.94; Found: C, 53.72; H, 2.51; N, 17.82%.

4.2. Biological evaluation

4.2.1. In vitro cytotoxic activity

The anti-proliferative activity of the synthesized compounds was assessed using MTT assay protocol [34,35,52]. A panel of human cancer cell lines namely; colorectal carcinoma (HCT-116), hepatocellular carcinoma (HepG2) and breast cancer (MCF-7) was used in this test. As we targeted the DNA and Topo II, doxorubicin as a potential intercalative Topo II inhibitor was used as a positive control. The cell lines were got from ATCC (American Type Culture Collection) via the Holding company for biological products and vaccines (VACSERA, Cairo, Egypt). The anti-proliferative activities of the tested compounds were determined quantitatively as follows:

At first, the cells were cultured into a medium of RPMI-1640 with 10% fetal bovine serum. Then, two different antibiotics were added at 37 °C in a 5% CO_2 incubator: penicillin (100 units/mL) and streptomycin (100 μg/mL). Next, we seeded the cells in a 96-well plate by a density of 1.0 × 10^4 cells / well at 37 °C for 48 h under 5% CO_2. The synthesized compounds with different concentrations were applied into the cell lines and incubated for 24 h. After 24 h, 20 μl of MTT solution (5 mg/mL) was added and incubated for 4 h. Then, DMSO (100 μl) was added into each well to dissolve the formed purple formazan. After that, a colorimetric assay was measured and recorded at absorbance of 570 nm using a plate reader (EXL 800, USA). The relative cell viability in percentage was calculated as (A570 of treated samples/A570 of untreated sample) × 100. Results for IC_{50}values of the active compounds were summarized in Table 2.

4.2.2. Measurement of topoisomerase II activity

The most active anti-proliferative members (**12, 15, 19, 21,** and **22**) were analyzed for their Topo II inhibitory activities. The reported method described by Patra et al. [53] was applied using Topo II drug screening kit (TopoGEN, Inc., Columbus). Doxorubicin was used as a positive control.

A typical enzyme reaction was structured to determine Topo II activity. The reaction mixture included Topo II (2 μl), substrate super coiled pHot1 DNA (0.25 μg), 50 μg/ml test compound (2 μl), and assay buffer (4 μl). To start the reaction, the mixture was allowed to incubate in 37 °C for 30 min. To terminate the reaction, a mixture of 10% sodium dodecylsulphate (2 μl) and proteinase K (50 μg/mL) was added at 37 °C for 15 min. then incubated for 15 min at 37 °C. After that, the DNA was run on 1% agarose gel in BioRad gel electrophoresis system for 1–2 h followed by staining with GelRedTM stain for 2 h and destained for 15 min with TAE buffer. The gel was imaged via BioRad's Gel DocTMEZ system. Both supercoiled and linear strands DNA were incorporated in the gel as markers for DNA-Topo II intercalators. The results of IC_{50} values were calculated using the GraphPad Prism version 7. Each reaction was performed in duplicate, and at least three independent determinations of each IC_{50} were made.

4.2.3. DNA/Methyl green assay

The most active anti-proliferative members (**12, 15, 19, 21,** and **22**) were evaluated for their DNA-binding affinities, using doxorubicin as a positive control according to methyl green dye method described by Burres et al. [38]. Activated Calf Thymus DNA (Merk, Germany) was treated with methyl green (Merk, Germany), then the synthesized compounds were applied to displace the methyl green dye, producing equivalent color. The results were reported as a 50% inhibition concentration values (IC_{50}) calculated by linear regression of data plotted on a semi-log scale and summarized in Table 3.

4.2.4. Flow cytometry analysis for cell cycle

To determine the role of the synthesized compounds in cell cycle distribution, cell cycle analysis was performed using propidium iodide (PI) staining and flow cytometry analysis for compound **22**. Flow Cytometry Kit for Cell Cycle Analysis (ab139418_Propidium Iodide Flow Cytometry Kit/BD) was used in this test. HepG2 cells were treated with compound **22** (2.81 μM) for 24 h. Then, the cells were fixed in 70% ethanol at 4 °C for 12 h. After that, the cells were washed with cold PBS, incubated with 100 μl RNase A at 37 °C for 30 min, and stained with 400 μl PI in the dark at room temperature for further 30 min. The stained cells were measured using Epics XL-MCL™ Flow Cytometer (Beckman Coulter), and the data were analyzed using Flowing software (version 2.5.1, Turku Centre for Biotechnology, Turku, Finland) [54].

4.2.5. Flow cytometry analysis for apoptosis

Flow cytometry cell apoptosis analysis was used to investigate the apoptotic effect of the synthesized compounds. HepG2 cells were treated with compound **22** (2.81 μM) for 24 h, collected by trypsin,

centrifuged, washed two successive times with PBS, suspended in 500 µl binding buffer, and double stained with 5 µl Annexin V-FITC and 5 µl PI in the dark at room temperature for 15 min. The stained cells were measured using Epics XL-MCL™ Flow Cytometer and analyzed using Flowing software [54].

4.2.6. Caspase-3 and caspase-9 activation assay

The percentage of caspase-3 and caspase-9 activation was determined using the Caspase- Invitrogen Caspase-3 ELISA Kit (KHO1091) and Invitrogen Caspase 9 Human ELISA Kit (BMS2025) following the manufacturer's instructions [55,56].

4.2.7. Statistical analyses

All data obtained from the biological evaluation studies are presented as mean ± SEM values and analyzed with unpaired student's *t*-test using GraphPad Prism version 7 (GraphPad Software, San Diego, CA), with $p < 0.05$ was considered statistically significant.

4.3. Docking studies

Docking studies were carried out utilizing discovery studio 4.0. The 3D crystal structure of the target macromolecule (DNA-topoisomerase II complex) was obtained from the protein databank (PDB ID: 4G0U, resolution: 2.7 Å).

At first, the co-crystallized ligand and water molecules were deleted from the DNA-topoisomerase II complex, leaving protein and DNA. Then, Valence monitor option was applied to correct any incorrect valence. Next, the energy of the complex was minimized by applying CHARMM and MMFF94 force fields [57–60]. After that, the active binding site was defined and prepared for docking. The structures of the synthesized compounds and doxorubicin were sketched using ChemBioDraw Ultra 14.0 and saved in MDL-SD file format. Next, the MDL-SD file was opened, 3D structures were protonated and the energy minimized by applying CHARMM and MMFF94 force fields then prepared for docking.

CDOCKER protocol was used for carrying out the docking studies. A maximum of 10 conformers was considered for each molecule in the docking analysis. Finally, the most ideal pose was selected according to its binding free energy with DNA–Topo II as well as its binding mode with the target molecule.

Declaration of Competing Interest

The authors declare that they have no known competing financial interests or personal relationships that could have appeared to influence the work reported in this paper.

Acknowledgment

The authors would like to acknowledge the extremely valuable suggestions and technical assistance made by Dr. Mohamed R. Elnagar, Department of Pharmacology and Toxicology, Faculty of Pharmacy, Al-Azhar University, Cairo, Egypt.

Appendix A. Supplementary material

Supplementary data to this article can be found online at https://doi.org/10.1016/j.bioorg.2020.104255.

References

[1] A. Remesh, Toxicities of anticancer drugs and its management, Ambili Remesh, Int. J. Basic Clin. Pharmacol. 1 (1) (2012) 2–12.
[2] T. Helleday, E. Petermann, C. Lundin, B. Hodgson, R.A. Sharma, DNA repair pathways as targets for cancer therapy, Nat. Rev. Cancer 8 (3) (2008) 193–204.
[3] A. Rescifina, C. Zagni, M.G. Varrica, V. Pistarà, A. Corsaro, Recent advances in small organic molecules as DNA intercalating agents: Synthesis, activity, and modeling, Eur. J. Med. Chem. 74 (2014) 95–115.
[4] M. Ibrahim, M. Taghour, A.M. Metwaly, A. Belal, A. Mehany, M. Elhendawy, M. Radwan, A. Yassin, N. El-Deeb, E. Hafez, Design, synthesis, molecular modeling and anti-proliferative evaluation of novel quinoxaline derivatives as potential DNA intercalators and topoisomerase II inhibitors, Eur. J. Med. Chem. 155 (2018) 117–134.
[5] T. Yokochi, K.D. Robertson, Doxorubicin inhibits DNMT1, resulting in conditional apoptosis, Mol. Pharmacol. 66 (6) (2004) 1415–1420.
[6] J.L. Nitiss, Targeting DNA topoisomerase II in cancer chemotherapy, Nat. Rev. Cancer 9 (5) (2009) 338–350.
[7] R. Martinez, L. Chacon-Garcia, The search of DNA-intercalators as antitumoral drugs: what it worked and what did not work, Curr. Med. Chem. 12 (2) (2005) 127–151.
[8] B.M. Zeglis, V.C. Pierre, J.K. Barton, Metallo-intercalators and metallo-insertors, Chem. Commun. (44) (2007) 4565–4579.
[9] M.R. Gill, J.A. Thomas, Ruthenium (II) polypyridyl complexes and DNA—from structural probes to cellular imaging and therapeutics, Chem. Soc. Rev. 41 (8) (2012) 3179–3192.
[10] F. Gago, Stacking interactions and intercalative DNA binding, Methods 14 (3) (1998) 277–292.
[11] J.C. Wang, Cellular roles of DNA topoisomerases: a molecular perspective, Nat. Rev. Mol. Cell Biol. 3 (6) (2002) 430–440.
[12] Y. Pommier, E. Leo, H. Zhang, C. Marchand, DNA topoisomerases and their poisoning by anticancer and antibacterial drugs, Chem. Biol. 17 (5) (2010) 421–433.
[13] L.F. Liu, DNA topoisomerase poisons as antitumor drugs, Annu. Rev. Biochem. 58 (1) (1989) 351–375.
[14] T.D. Shenkenberg, D.D. Von Hoff, Mitoxantrone: a new anticancer drug with significant clinical activity, Ann. Intern. Med. 105 (1) (1986) 67–81.
[15] A. Chilin, G. Marzaro, C. Marzano, L. Dalla Via, M.G. Ferlin, G. Pastorini, A. Guiotto, Synthesis and antitumor activity of novel amsacrine analogs: the critical role of the acridine moiety in determining their biological activity, Biorg. Med. Chem. 17 (2) (2009) 523–529.
[16] C. Avendaño, J. Menéndez, Medicinal chemistry of anticancer agents, Elsevier, Amsterdam, 2008.
[17] I.H. Eissa, A.M. Metwaly, A. Belal, A.B. Mehany, R.R. Ayyad, K. El-Adl, H.A. Mahdy, M.S. Taghour, K.M. El-Gamal, M.E. El-Sawah, Discovery and antiproliferative evaluation of new quinoxalines as potential DNA intercalators and topoisomerase II inhibitors, Arch. Pharm. 352 (11) (2019) 1900123.
[18] W.M. Eldehna, M.F. Abo-Ashour, A. Nocentini, P. Gratteri, I.H. Eissa, M. Fares, O.E. Ismael, H.A. Ghabbour, M.M. Elaasser, H.A. Abdel-Aziz, Novel 4/3-((4-oxo-5-(2-oxoindolin-3-ylidene) thiazolidin-2-ylidene) amino) benzenesulfonamides: Synthesis, carbonic anhydrase inhibitory activity, anticancer activity and molecular modelling studies, Eur. J. Med. Chem. 139 (2017) 250–262.
[19] A.A. Gaber, A.H. Bayoumi, A.M. El-morsy, F.F. Sherbiny, A.B. Mehany, I.H. Eissa, Design, synthesis and anticancer evaluation of 1H-pyrazolo [3, 4-d] pyrimidine derivatives as potent EGFR WT and EGFR T790M inhibitors and apoptosis inducers, Bioorg. Chem. 80 (2018) 375–395.
[20] A.M. El-Naggar, M.M. Abou-El-Regal, S.A. El-Metwally, F.F. Sherbiny, I.H. Eissa, Synthesis, characterization and molecular docking studies of thiouracil derivatives as potent thymidylate synthase inhibitors and potential anticancer agents, Mol. Divers 21 (4) (2017) 967–983.
[21] S.A. Elmetwally, K.F. Saied, I.H. Eissa, E.B. Elkaeed, Design, synthesis and anticancer evaluation of thieno [2, 3-d] pyrimidine derivatives as dual EGFR/HER2 inhibitors and apoptosis inducers, Bioorg. Chem. 88 (2019) 102944.
[22] H.A. Mahdy, M.K. Ibrahim, A.M. Metwaly, A. Belal, A.B. Mehany, K.M. El-Gamal, A. El-Sharkawy, M.A. Elhendawy, M.M. Radwan, M.A. Elsohly, Design, synthesis, molecular modeling, in vivo studies and anticancer evaluation of quinazolin-4 (3H)-one derivatives as potential VEGFR-2 inhibitors and apoptosis inducers, Bioorg. Chem. (2019) 103422.
[23] I.H. Eissa, A.M. El-Naggar, M.A. El-Hashash, Design, synthesis, molecular modeling and biological evaluation of novel 1H-pyrazolo [3, 4-b] pyridine derivatives as potential anticancer agents, Bioorg. Chem. 67 (2016) 43–56.
[24] I.H. Eissa, A.M. El-Naggar, N.E. El-Sattar, A.S. Youssef, Design and discovery of novel quinoxaline derivatives as dual DNA intercalators and topoisomerase II inhibitors, Anticancer Agents Med. Chem 18 (2) (2018) 195–209.
[25] D.E. Graves, L.M. Velea, Intercalative binding of small molecules to nucleic acids, Curr. Org. Chem. 4 (9) (2000) 915–929.
[26] G. Minotti, P. Menna, E. Salvatorelli, G. Cairo, L. Gianni, Anthracyclines: molecular advances and pharmacologic developments in antitumor activity and cardiotoxicity, Pharmacol. Rev. 56 (2) (2004) 185–229.
[27] J. Gallego, A.R. Ortiz, B. de Pascual-Teresa, F. Gago, Structure–affinity relationships for the binding of actinomycin D to DNA, J. Comput. Aided Mol. Des. 11 (2) (1997) 114–128.
[28] S.A. Bailey, D.E. Graves, R. Rill, Binding of actinomycin D to the T (G) nT motif of double-stranded DNA: determination of the guanine requirement in nonclassical, non-GpC binding sites, Biochemistry 33 (38) (1994) 11493–11500.
[29] K.A. Abouzid, G.H. Al-Ansary, A.M. El-Naggar, Eco-friendly synthesis of novel cyanopyridine derivatives and their anticancer and PIM-1 kinase inhibitory activities, Eur. J. Med. Chem. 134 (2017) 357–365.
[30] A.M. El-Naggar, M.M. Hemdan, S.R. Atta-Allah, An efficient one-pot synthesis of new Coumarin derivatives as potent anticancer agents under microwave irradiation, J. Heterocyclic Chem. 54 (6) (2017) 3519–3526.
[31] S.A. El-Metwally, A.K. Khalil, A.M. El-Naggar, W.M. El-Sayed, Novel tetrahydrobenzo [b] thiophene compounds exhibit anticancer activity through enhancing apoptosis and inhibiting tyrosine kinase, Anticancer Agents Med. Chem. 18 (12) (2018) 1761–1769.

[32] A.M. El-Naggar, A.K. Khalil, H.M. Zeidan, W.M. El-Sayed, Eco-friendly synthesis of pyrido [2, 3-d] pyrimidine analogs and their anticancer and tyrosine kinase inhibition activities, Anticancer Agents Med. Chem. 17 (12) (2017) 1644–1651.
[33] C.A. Obafemi, W. Pfleiderer, Permanganate oxidation of quinoxaline and its derivatives, Helv. Chim. Acta 77 (6) (1994) 1549–1556.
[34] T. Mosmann, Rapid colorimetric assay for cellular growth and survival: application to proliferation and cytotoxicity assays, J. Immunol. Methods 65 (1–2) (1983) 55–63.
[35] F. Denizot, R. Lang, Rapid colorimetric assay for cell growth and survival: modifications to the tetrazolium dye procedure giving improved sensitivity and reliability, J. Immunol. Methods 89 (2) (1986) 271–277.
[36] M. Thabrew, R.D. Hughes, I.G. Mcfarlane, Screening of hepatoprotective plant components using a HepG2 cell cytotoxicity assay, J. Pharm. Pharmacol. 49 (11) (1997) 1132–1135.
[37] P. Furet, G. Caravatti, N. Lydon, J.P. Priestle, J.M. Sowadski, U. Trinks, P. Traxler, Modelling study of protein kinase inhibitors: binding mode of staurosporine and origin of the selectivity of CGP 52411, J. Comput. Aided Mol. Des. 9 (6) (1995) 465–472.
[38] N.S. Burres, A. Frigo, R.R. Rasmussen, J.B. McAlpine, A colorimetric microassay for the detection of agents that interact with DNA, J. Nat. Prod. 55 (11) (1992) 1582–1587.
[39] B. Pucci, M. Kasten, A. Giordano, Cell cycle and apoptosis, Neoplasia (New York, NY) 2 (4) (2000) 291.
[40] W.M. Eldehna, G.S. Hassan, S.T. Al-Rashood, T. Al-Warhi, A.E. Altyar, H.M. Alkahtani, A.A. Almehizia, H.A. Abdel-Aziz, Synthesis and in vitro anticancer activity of certain novel 1-(2-methyl-6-arylpyridin-3-yl)-3-phenylureas as apoptosis-inducing agents, J. Enzyme Inhib. Med. Chem. 34 (1) (2019) 322–332.
[41] A. Sabt, O.M. Abdelhafez, R.S. El-Haggar, H.M. Madkour, W.M. Eldehna, E.E.-D.A. El-Khrisy, M.A. Abdel-Rahman, L.A. Rashed, Novel coumarin-6-sulfonamides as apoptotic anti-proliferative agents: synthesis, in vitro biological evaluation, and QSAR studies, J. Enzyme Inhib. Med. Chem. 33 (1) (2018) 1095–1107.
[42] W. Naowaratwattana, W. De-Eknamkul, E.G. De Mejia, Phenolic-containing organic extracts of mulberry (Morus alba L.) leaves inhibit HepG2 hepatoma cells through G2/M phase arrest, induction of apoptosis, and inhibition of topoisomerase IIα activity, J. Med. Food 13 (5) (2010) 1045–1056.
[43] G.M. Cohen, Caspases: the executioners of apoptosis, Biochem. J. 326 (1) (1997) 1–16.
[44] W.M. Eldehna, M.F. Abo-Ashour, H.S. Ibrahim, G.H. Al-Ansary, H.A. Ghabbour, M.M. Elaasser, H.Y. Ahmed, N.A. Safwat, Novel [(3-indolylmethylene) hydrazono] indolin-2-ones as apoptotic anti-proliferative agents: design, synthesis and in vitro biological evaluation, J. Enzyme Inhib. Med. Chem. 33 (1) (2018) 686–700.
[45] S.T. Al-Rashood, A.R. Hamed, G.S. Hassan, H.M. Alkahtani, A.A. Almehizia, A. Alharbi, M.M. Al-Sanea, W.M. Eldehna, Antitumor properties of certain spirooxindoles towards hepatocellular carcinoma endowed with antioxidant activity, J. Enzyme Inhib. Med. Chem. 35 (1) (2020) 831–839.
[46] A.G. Porter, R.U. Jänicke, Emerging roles of caspase-3 in apoptosis, Cell Death Differ. 6 (2) (1999) 99–104.
[47] D.R. McIlwain, T. Berger, T.W. Mak, Caspase functions in cell death and disease, Cold Spring Harb. Perspect. Biol. 5 (4) (2013) a008656.
[48] G. Yeoh, S. Barton, K. Kaestner, Int. J. Biochem. Cell Biol. 43 (2) (2011) 172.
[49] A. Kumar, U. Bora, Molecular docking studies of curcumin natural derivatives with DNA topoisomerase I and II-DNA complexes, Interdiscipl. Sci. Comput. Life Sci. 6 (4) (2014) 285–291.
[50] D.R. Romer, Synthesis of 2, 3-dichloroquinoxalines via Vilsmeier reagent chlorination, J. Heterocycl. Chem. 46 (2) (2009) 317–319.
[51] O.O. Ajani, C.A. Obafemi, C.O. Ikpo, K.O. Ajanaku, K.O. Ogunniran, O.O. James, Comparative study of microwave assisted and conventional synthesis of novel 2-quinoxalinone-3-hydrazone derivatives and its spectroscopic properties, Int. J. Phys. Sci. 4 (4) (2009) 156–164.
[52] M.I. Thabrew, R.D. Hughes, I.G. Mcfarlane, Screening of hepatoprotective plant components using a HepG2 cell cytotoxicity assay, J. Pharm. Pharmaco. 49 (11) (1997) 1132–1135.
[53] M.-K. Ibrahim, A.A. Abd-Elrahman, R.R. Ayyad, K. El-Adl, A.M. Mansour, I.H. Eissa, Design and synthesis of some novel 2-(3-methyl-2-oxoquinoxalin-1 (2H)-yl)-N-(4-(substituted) phenyl) acetamide derivatives for biological evaluation as anticonvulsant agents, Bull Fac. Pharm. Cairo Univ. 51 (1) (2013) 101–111.
[54] R.I. Jenie, S. Handayani, R.A. Susidarti, L.Z. Udin, E. Meiyanto, The cytotoxic and antimigratory activity of Brazilin-doxorubicin on MCF-7/HER2 cells, Adv. Pharm. Bull. 8 (3) (2018) 507.
[55] S. Sudan, H.V. Rupasinghe, Flavonoid-enriched apple fraction AF4 induces cell cycle arrest, DNA topoisomerase II inhibition, and apoptosis in human liver cancer HepG2 cells, Nutr. Cancer 66 (7) (2014) 1237–1246.
[56] A.M. Bruynzeel, M.A. Abou El Hassan, E. Torun, A. Bast, W.J. van der Vijgh, F.A. Kruyt, Caspase-dependent and-independent suppression of apoptosis by monoHER in Doxorubicin treated cells, Br. J. Cancer 96 (3) (2007) 450–456.
[57] A.G.A. El-Helby, R.R. Ayyad, H.M. Sakr, A.S. Abdelrahim, K. El-Adl, F.S. Sherbiny, I.H. Eissa, M.M. Khalifa, Design, synthesis, molecular modeling and biological evaluation of novel 2, 3-dihydrophthalazine-1, 4-dione derivatives as potential anticonvulsant agents, J. Mol. Struct. 1130 (2017) 333–351.
[58] M.K. Ibrahim, I.H. Eissa, M.S. Alesawy, A.M. Metwaly, M.M. Radwan, M.A. ElSohly, Design, synthesis, molecular modeling and anti-hyperglycemic evaluation of quinazolin-4 (3H)-one derivatives as potential PPARγ and SUR agonists, Biorg. Med. Chem. 25 (17) (2017) 4723–4744.
[59] K.M. El-Gamal, A.M. El-Morsy, A.M. Saad, I.H. Eissa, M. Alswah, Synthesis, docking, QSAR, ADMET and antimicrobial evaluation of new quinoline-3-carbonitrile derivatives as potential DNA-gyrase inhibitors, J. Mol. Struct. 1166 (2018) 15–33.
[60] M.I. Youssef, Y. Zhou, I.H. Eissa, Y. Wang, J. Zhang, L. Jiang, W. Hu, J. Qi, Z. Chen, Tetradecyl 2, 3-dihydroxybenzoate alleviates oligodendrocyte damage following chronic cerebral hypoperfusion through IGF-1 receptor, Neurochem. Int. 138 (2020) 104749.